POLITECNICO DI TORINO

DOCTORAL SCHOOL (SCUDO)

Ph.D. in Water and Land Management Engineering

XXV Doctoral Cycle

Ph.D. Dissertation

Impact of hyporheic zones
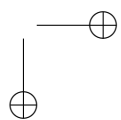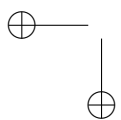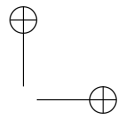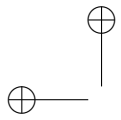# on nutrient dynamics

Laura BARDINI

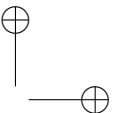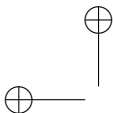| **Tutors**	**Doctoral School Coordinator**
Prof. Luca Ridolfi	
Prof. Roberto Revelli	Prof. Claudio Scavia
Eng. Fulvio Boano	

20 March 2013

Acknowledgements

This thesis is the result of the research work of the last three years, which represented to me a very interesting work and life experience. For this reason I would like to thank all the people who, both scientifically and emotionally, contributed to the achievement of my objective.

Firstly, I thank my tutors, Luca Ridolfi, Roberto Revelli and Fulvio Boano, who followed me in these three years supporting me, and giving me precious advices and the possibility to do a reserch experience abroad.

About this, I want to say thank you to professor Bayani Cardenas for having been so helpful in the period I spent in Texas and also for his contribute to my research project. Thanks also to Kuldeep, Lichun and Peter who made me feel at home in Texas and made me spend an unforgettable "american" birthday.

I thank all my colleagues for continuously providing me comprehension, support, laughs and many essential coffee breaks. Some of them are very special to me but I would like to thank all in "order of appearance": thanks Stefania G., Riccardo, Roberta, Stefania S., Elisa B., Claudia, Fabio, Stefano T., Stefania B., Francesco, Laura, Claudia, Pum, Filippo, Daniele, Paolo, Stefania T., Alessandro, Anacleto, Andrea C., Marco, Stefano F., Roberto, Andrea G., Anna, Alberto P., Alberto C., Uzair, Azmat, Julia, Luca, Luigi ed Elisa M.

Thanks to my long-time special friends Elena, Sabrina and Sara for being always beside me in the important moments of my life.

Thanks also to Luca and Giorgio for the funny times spent together.

At least, a very special thank to Marco and my family, my grandma Vilma, my mom Francesca, my dad Luciano and my sister Chiara for always encouraging and standing me. I am proud of them and I hope this thesis will make them a little proud of me too.
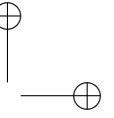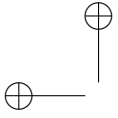

Questa tesi rappresenta il frutto del lavoro di ricerca degli ultimi tre anni, che hanno rappresentato per me un'interessante esperienza lavorativa ma soprattutto di vita. Per questo motivo ci tengo a ringraziare tutte le persone che mi hanno accompagnato in questo percorso, contribuendo, scientificamente o emotivamente, al raggiungimento del mio obiettivo.

Il primo grazie va ai miei tutori, Luca Ridolfi, Roberto Revelli e Fulvio Boano, che mi hanno seguito in questi tre anni incoraggiandomi, dandomi consigli preziosi e offrendomi la possibilità di fare un'esperienza di ricerca all'estero.
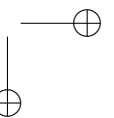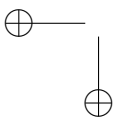
A questo proposito, voglio ringraziare il professor Bayani Cardenas per la disponibilità che ha dimostrato nei miei confronti nei tre mesi passati in Texas e per il contributo che ha dato alla mia ricerca. Grazie anche a Kuldeep, Lichun e Peter per avermi fatto sentire come a casa in Texas ed avermi fatto passare un indimenticabile compleanno "americano".
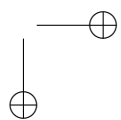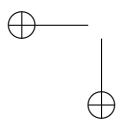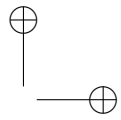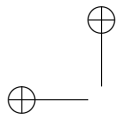
Grazie ai miei colleghi per darmi continuamente comprensione, leggerezza, sostegno, risate e tante fondamentali pause caffè. Con alcuni ho creato un rapporto davvero speciale ma ci tengo a ringraziarli tutti, "in ordine di apparizione": grazie a Stefania G., Riccardo, Roberta, Stefania S., Elisa B., Claudia, Fabio, Stefano T., Stefania B., Francesco, Laura, Claudia, Pum, Filippo, Daniele, Paolo, Stefania T., Alessandro, Anacleto, Andrea C., Marco, Stefano F., Roberto, Andrea G., Anna, Alberto P., Alberto C., Uzair, Azmat, Julia, Luca, Luigi ed Elisa M.

IV

Contents

Introduction

Riverine systems are vital for the environment health and for the economic and social life of countries. Channels preserve ecosystem biodiversity by providing habitats for a large variety of animals and plants and they also act in water and nutrient cycling. Rivers were essential for the development of civilitation and economy and, even today, they represent sources of food, fresh water and energy, via hydroelectric plants, and they are used for navigation. Their important function is also recognized by the European Union that established a Community framework, the Water Framework Directive (WFD; 2000/60/EC), supporting a new integrated approach for the protection, management and sustainable use of water bodies. In this context, the study of pollutant distribution in the riverine ecosystem and, in particular, of surface and subsurface water interactions, becomes fundamental and can lead to a better preservation of river and aquifer quality, ecosystem biodiversity and human health.

Solute transport along a river is a complex process due to the occurrence of different transport and exchange mechanisms. Turbulent water flow, together with variations in bed topography, drives water exchange between the river and the subsurface environment with a very wide range of spatial and temporal scales (Cardenas, 2008b; Stonedahl et al., 2010). Small-scale exchange flow is mainly induced by bedforms like ripples and dunes (Elliott and Brooks, 1997b,a; Packman and Brooks, 2001; Packman et al., 2004; Boano et al., 2007b; Cardenas and Wilson, 2007c), while large-scale exchange flows depend on larger geomorphological features (Boano et al., 2006a; Tonina and Buffington, 2007; Cardenas, 2008a; Revelli et al., 2008). The picture is further complicated by the fact that exchange processes at different scales interact and
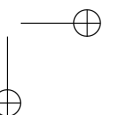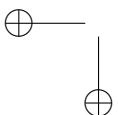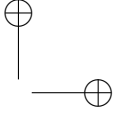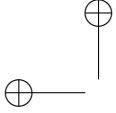
determine complex system of nested flow cells (Stonedahl et al., 2010). The exchange of water and solutes across the riverbed and the river banks affects the ecology of the fluvial environment since it contributes to the connection of surface and subsurface waters, whose physical and chemical characteristics are very different. The exchange region, located beneath and adjacent to the river, is the "hyporheic zone".

The water-borne solute spatial distribution in this zone is due to the interplay of hydrological and biogeochemical processes. In fact, several intense biogeochemical reactions, mediated by microbial communities, occur in hyporheic sediments (Storey et al., 1999; Fischer and Pusch, 2001; Fischer et al., 2005). Water-borne chemicals entering hyporheic sediments are transformed into oxidized or reduced forms before being released back to the river. In particular, organic substances are used as electron donors in a series of redox reactions, with different electron acceptors, e.g., oxygen and nitrate (Hunter et al., 1998). These sediment-scale transformations have proved to play a significant role in nutrient cycling and for the pollutant attenuation in fluvial ecosystems (e.g., Findlay, 1995; Brunke and Gonser, 1997; Boulton et al., 1998; Tonina and Buffington, 2009; Wondzell, 2011). However, hyporheic biogeochemical reactions may also lead to a net nitrate production and release into the river or to the transformation of pollutants into other dangerous compounds. Thus, it becomes important to deeply investigate the processes occurring in the hyporheic zone, in order to take them into account in projects of river management or rehabilitation and contamination risk assessment.

In the last decades several researchers investigated the interaction of hydrology and biogeochemistry in the hyporheic zone, at both small and large spatial scales, with different methodological approaches (Jones and Mulholland, 2000), such as direct measurements (Duff et al., 2000; Westhoff et al., 2011), reach-scale tracer tests (e.g., Bencala and Walters, 1983; Gooseff et al., 2013) or physically-based models (e.g., Elliott and Brooks, 1997b). However, we are still far a complete understanding of this complex topic. Furthermore, due to the complexity of this topic, most of the models, which take into account both hydrological and chemical processes, assume the homogeneity of sediment properties. However, in some cases, sediment heterogeneity can lead to the presence

of the so called "hot spots", where higher reaction rates than the surrounding area occur (McClain et al., 2003).

The aim of this thesis is to study the impact of small-scale exchange fluxes and microbial reactions on the spatial distribution of four chemicals in the hyporheic zone. In particular, we choose dissolved organic carbon, oxygen, nitrate and ammonium, which usually present high concentrations in rivers, as a consequence of anthropogenic activities (Boyer et al., 2006; Mulholland et al., 2008). In order to do this, we will develop a numerical model to simulate hyporheic fluxes and solute concentrations in duned and rippled streambeds, that represent typical widespread configurations in riverine environments, and we will investigate the effect of hydraulic, physical and chemical properties of the sediments. In the second part, we will use the model for estimating the influence of small-scale permeability heterogeneity on the dynamics of the reactive solutes object of study.

The work is divided into three Chapters. Chapter 1 presents a review of the last works involving the hyporheic zone, with a description of the main ecological, hydrological and biogeochemical approaches. The attention is then focused on the driving mechanisms of hyporheic fluxes and the main methodologies used for the estimation of surface and subsurface water exchanges. Models and field studies of reactive solute transport are also discussed.

Chapter 2 introduces the biogeochemical two-dimensional model. The hyporheic biochemical reactions are coupled with the hyporheic advective flow field, induced by the presence of stream dunes, and the dispersive fluxes, caused by hydrodynamic dispersion, for modeling the reactive solute spatial distribution. Sensitivity analyses of hydraulic, chemical and hydrological parameters are also performed. In particular, the effect of stream velocity, surface water chemistry and sediment permeability on solute dynamics is investigated.

Chapter 3 deals with hyporheic water exchanges within two different rippled streambeds. The study is focused on the impact of small-scale variations in sediment hydraulic properties on the hyporheic chemical zonation. Numerical flow and reactive transport simulations are performed for two realistic heterogeneous permeability cases, typical of lowland rivers, and two equivalent homogeneous cases. The resulting chemical distributions are then
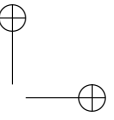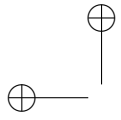
compared in order to analyze the impact of sediment permeability heterogeneity on bulk reaction rates and nutrient sink/source function of the streambed.
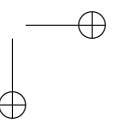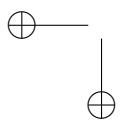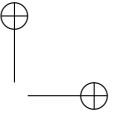
Chapter 1

Hyporheic zone: state of art

1.1 Introduction

The hyporheic zone is the transitional zone between the stream and the aquifer (Figure 1.1), characterized by

- active surface and subsurface water exchange,

- intense biogeochemical activity,

- a characteristic fauna of invertebrates and microorganisms, defined as "hyporheos" by Williams and Hynes (1974).

These peculiarities make it a unique zone, from both hydrological, hydrogeological, biogeochemical and ecological points of view. For this reason, the hyporheic zone is not related to a single discipline but it was studied in the last decades with different scientific approaches. Figure 1.2 shows the conceptual model of the hyporheic zone for the disciplines of ecology, hydrology and hydrogeology. Ecology concentrates on the role of the hyporheic zone as a habitat and refuge for freshwater invertebrate fauna and as a location for salmonid egg development (Figure 1.2a) while hydrology focuses on the processes controlling water exchange through the streambed (Figure 1.2b). Lastly, hydrogeology studies the hyporheic zone as part of the groundwater system and considers as key aspects the
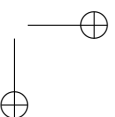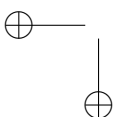
high Total Organic Carbon (TOC) content and the variety of the microbial community in the hyporheic sediments (Figure 1.2c).

The "hyporheic" term derives from the greek words "hypo" (i.e., "under") and "rheos" (i.e., "stream") and it literally means "under the stream". The adjective was coined by the ecologist Orghidan (1959) in order to describe the particular biotope[1], with unique physicochemical and biological conditions, previously discovered and studied by Chappuis (1942) and Angelier (1953). Based on field studies, Orghidan (1959) investigated the variegated nature of the hyporheic biota[2], which include surface organisms fully adapted to subsurface life, and he described the hyporheic biotope as an intermediate zone with both stream and aquifer physical and chemical characteristics (Kaeser, 2010).
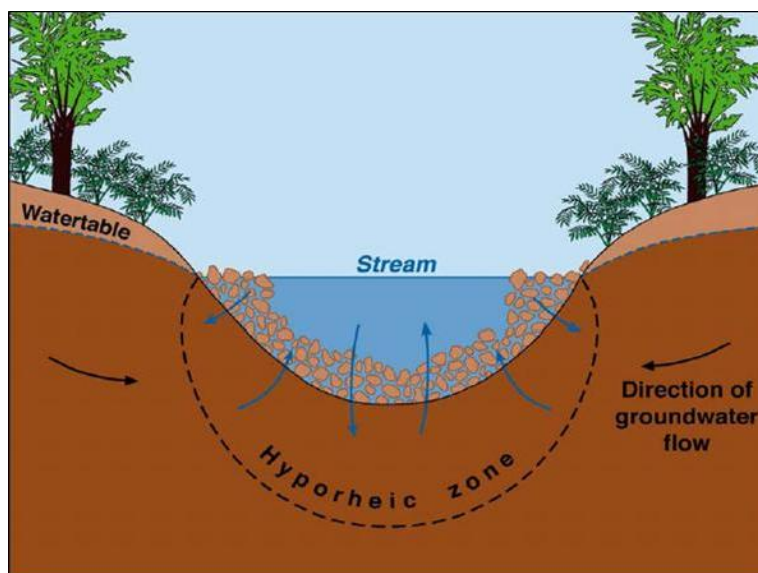
Figure 1.1: Illustrative representation of the hyporheic zone (from Alley et al., 2002).

---

[1] Area of uniform environmental conditions providing a living place for a specific biological community.

[2] The combined flora and fauna of a region.
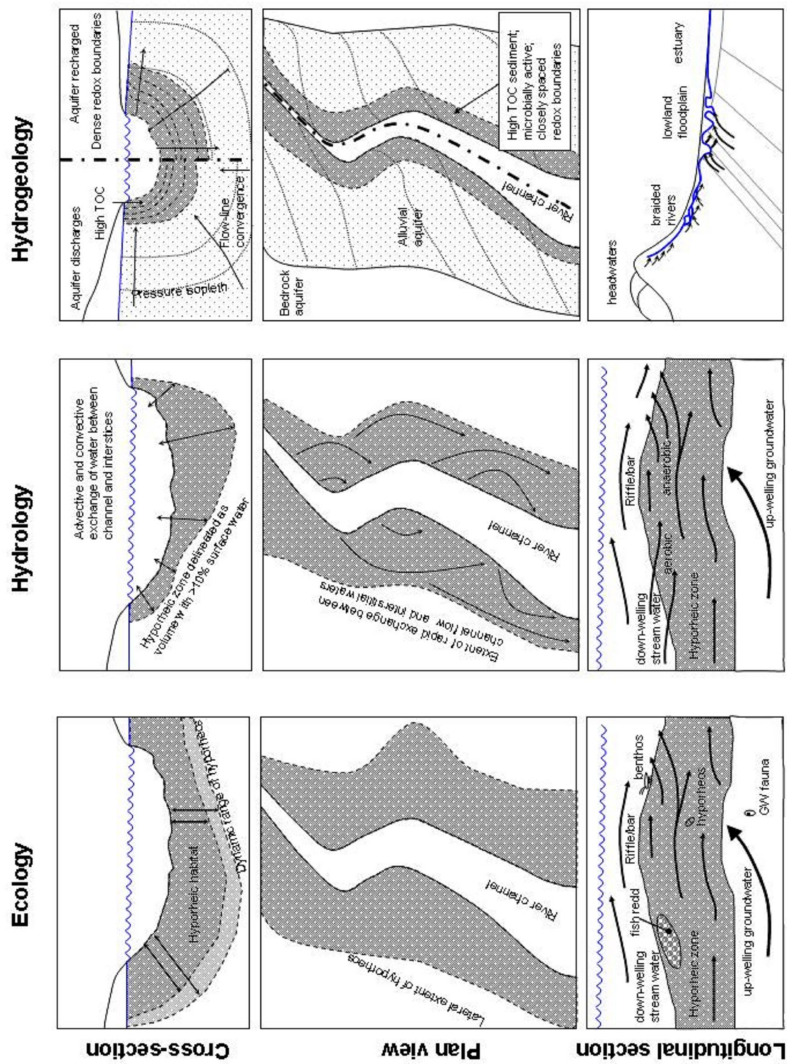
Figure 1.2: Conceptual models of the hyporheic zone for ecology, hydrology and hydrogeology disciplines (from Smith, 2005).

7

Brunke and Gonser (1997) underlined that, despite the direct connection with the stream, the hyporheic zone keeps lower oxygen concentrations than the saturation value, permanent darkness conditions, lower flow velocities and smaller daily and annual temperature fluctuations. Instead, Hatch et al. (2010) and Lautz and Fanelli (2008) found higher flow velocities, higher temperature fluctuations, steeper physical and chemical gradients and higher habitat diversity and productivity in the hyporheic zone in comparison to the groundwater environment. Thus, the hyporheic zone can be considered as a distinct ecotone[3] (Williams et al., 2010) with intermediate conditions between surface and subsurface waters (see Table 1.1 from Krause et al. (2011)). According to the surface and subsurface water mixing ratio, Triska et al. (1989) distinguished two different zones inside the hyporheic region by using tracer experiments. The "surface hyporheic zone", just beneath the river, was composed of more than 98% of surface water, while the "interactive hyporheic zone" included between 10% and 98% of surface water and gradients of nutrients and dissolved gases. This detailed distinction was no longer considered in further studies due to the difficult localization of the boundary between the two zones and the scarse spatial and temporal flexibility of the model (Vervier et al., 1992). Indeed, the hyporheic zone is a temporally and spatially dynamic ecotone, whose boundaries are continuously in evolution and, thus, difficult to define).

Ecologists identify the upper boundary of the hyporheic zone by the decline of light and flow velocity and they locate it beneath the benthic zone[4] at depths from few centimeters to tens of centimeters (Schwoerbel, 1964). The boundary between the hyporheic zone and the groundwater enviroment is difficult to establish, because of the variability in time of the connecting hydrological processes.

---

[3]Transition zone between two habitats, where two communities meet and integrate.

[4]Ecological region at the bottom of a body of water, including sediment surface and some sub-surface layers

Table 1.1: Summary of comparative physical and biological characteristics of groundwater, hyporheic and surface water environments (from Krause et al., 2011)

	Descriptive characteristic of environment		
	Groundwater	Hyporheos	Surface water
Physical characteristic			
Light	Constant darkness	Constant darkness	Daylight fluctuations
Current velocity	Low	Intermediate	High
Annual and daily temperature range	Very low	Low	High
Substrate stability	High	Intermediate	Low
Gradient of physico-chemical parameters	Low	Steep	Steep
Biological characteristics			
Habitat diversity	Low	Intermediate	High
Food-webs	Simple and short	Intermediate	Complex and long
Productivity	Low	Intermediate	High

9

Furthermore, single biotic[5] and abiotic[6] indicators cannot be used, since they do not take into account all the involved ecological aspects (Brunke and Gonser, 1997). Palmer (1993) suggested to leave to the single reasearchers the task to describe the boundaries of the water system object of study. Ecology literature reports cases of relatively shallow hyporheic zones, from few centimeters to some meters of depth, but Stanford and Ward (1988) and Danielopol (1989) observed the presence of riverine animals some kilometers beneath the river in flood-plain aquifers associated to large unregulated fluvial systems. About the horizontal extent of the hyporheic zone, Stanford and Ward (1993) introduced the "hyporheic corridor" concept in alluvial rivers, suggesting a longitudinal continuum of the hyporheic habitat along the river channel, with different depths, depending on floodplain geomorphology. Depth values were found to increase from headwater streams to intermediate reaches and to decline in lowland reaches (see Figures 1.3 and 1.4).

In hydrology literature, most researchers reported relatively shallow hyporheic zones (10-20 cm depth) but some studies also analyzed a deeper infiltration of stream water into sediments, up to several meters of depth (Puckett et al., 2008). In some cases the hyporheic zone laterally extended into the riparian zone, including paleo-channels and the wider floodplain, providing a significant spatially distributed habitat (Stanford and Ward, 1993; Woessner, 2000). Hydrologists define the size of the hyporheic zone based on water exchange flow paths and conservative solute residence times in the streambed. Water exchanges through the streambed occur at a very wide range of spatial and temporal scales, in response to variations in discharge, ambient groundwater flow, bed topography and permeability. Small streambed geomorphologic features, like ripples and dunes, induce small-scale exchanges, with short flow paths and small residence times (e.g., a few minutes), while larger features, like pool-riffle pairs, step-pool sequences or meander bends, cause large-scale exchanges, with longer flow paths and bigger residence times (e.g., some days, as seen by Kasahara and Wondzell, 2003, or up to years). These water and solute exchanges

---

[5]Living components.

[6]Non-living components.
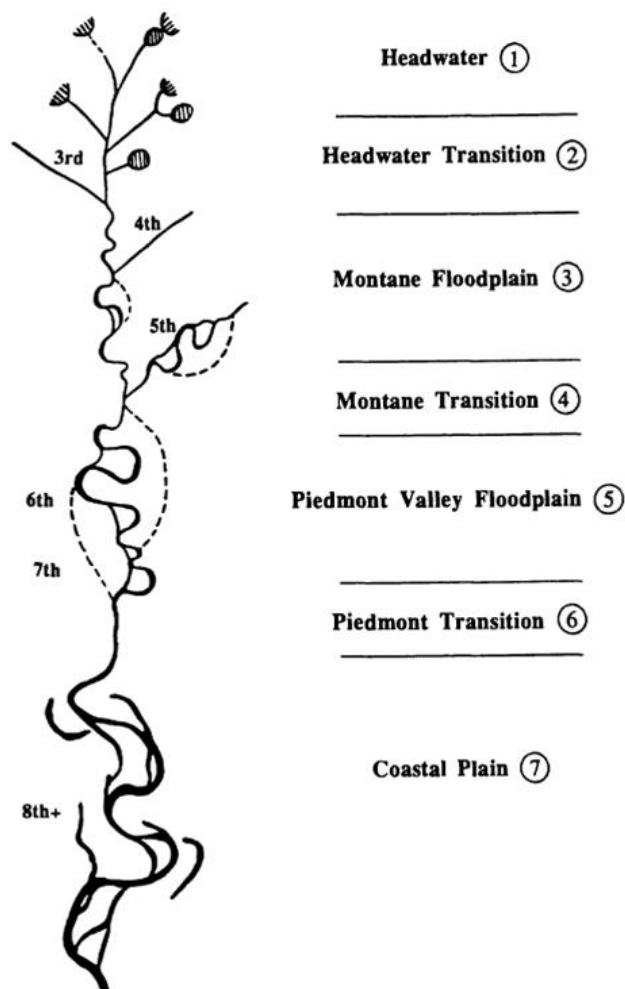
Figure 1.3: The hyporheic corridor of the river continuum (from Stanford and Ward, 1993).

through the streambed play an important role on the ecology of the fluvial environment. Upwelling subsurface water supplies stream organisms with nutrients, while downwelling stream water provides dissolved oxygen and organic matter to microbes and invertebrates in the hyporheic zone (Boulton et al., 1998). The mixing between waters with different temperatures and chemical compositions also

11
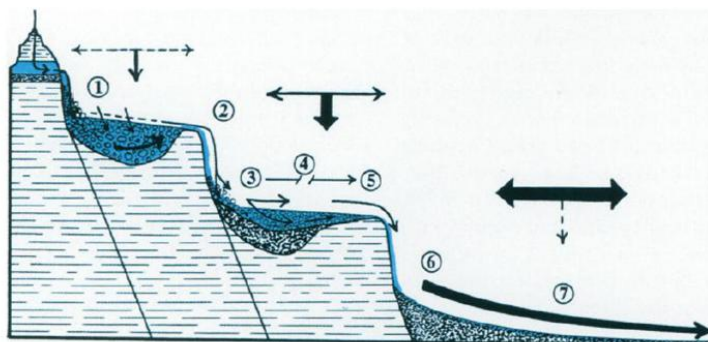
Figure 1.4: Cross-sectional representation of the hyporheic corridor (from Stanford and Ward, 1993). Surface and interstitial flows are represented by arrows, and numbers refer to segments identified in Figure 1.3. Vectors above the floodplains represent relative volume of annual overland (horizontal arrows) versus interstitial (vertical arrows) flow for these floodplains.

facilitates microbial diversity (Hedin et al., 1998) and the moderation of stream water temperature. The latter, in turn, has an influence on stream chemical reactions, development of aquatic organisms and speed and direction of fish migration (Jonsson, 1991; Prchalova et al., 2011). The hyporheic zone also provide a rooting zone for aquatic plants and thermal refugia for macroinvertebrates and other aquatic organisms (Burkholder et al., 2008). Besides, hyporheic sediments typically host intense biogeochemical activity, that can contribute to the natural attenuation or removal of pollutants and influences nutrient cyclings. In fact, water-borne solutes entering the sediments are transformed into oxidized or reduced substances by reactions mediated by hyporheic bacteria. In particular, organic substances can be used as electron donors in a series of redox reactions, with different electron acceptors, e.g., oxygen and nitrate. Other secondary reactions, like nitrification, also occur as soon as water enters the streambed. These pore-scale transformations concur to affect subsurface solute concentrations and, consequently, the chemistry of upwelling water and the quality of the stream environment. For example, Bohlke et al. (2009)

demonstrated with field measurements that hyporheic denitrification contributes substantially to nitrate removal in streams. This central function of the hyporheic zone is the subject of this thesis, and it is further discussed in section 2.3 and in the reminder of this work.

1.2   Water flows and exchanges

The hyporheic fluxes occur generally in response to variations in bed topography and permeability (Malard et al., 2002; Tonina and Buffington, 2009), with a very wide range of spatial and temporal scales (Figure 1.5). Large-scale exchanges depend on larger geomorphological features, like pool-riffle pairs (Tonina and Buffington, 2007), step-pool sequences (Harvey and Bencala, 1993) or meander bends (Boano et al., 2006a; Cardenas, 2008a; Revelli et al., 2008) while small-scale exchanges are mainly induced by river bed forms, like ripples and dunes (Elliott and Brooks, 1997b,a; Packman and Brooks, 2001; Packman et al., 2004; Gooseff et al., 2006; Boano et al., 2007b; Cardenas and Wilson, 2007a). Biological factors also contribute to enhance water exchange across
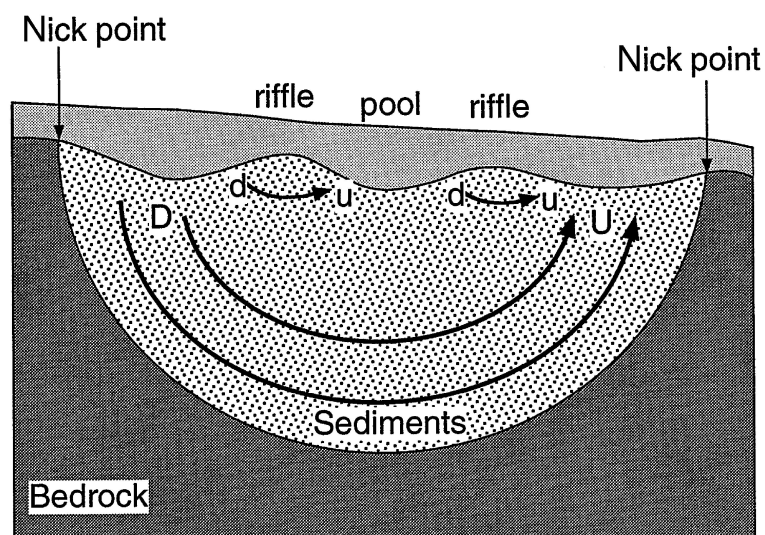
Figure 1.5: Small-scale and large-scale hyporheic exchanges (from Brunke and Gonser, 1997).

the streambed. In fact, the burrowing and feeding activities of benthic organisms result in an increase of pore size in the sediments, leading to higher vertical hydraulic conductivities (Boudreau, 2000; Song et al., 2007). Furthermore, transpiration by riparian vegetation enlarges hyporheic flow paths during the day and decreases them at night (Wondzell et al., 2010).

In the last decades three main methods were used for studying and quantifying hyporheic exchanges, i.e., field measurements, stream tracer tests, combined with stream transport models, and physically-based models.

The first approach consists of detailed field measurements of the topographical, hydraulic and physical characteristics of the site of interest, such as pressure head and/or temperature gradients, in order to assess the rate and the extent of hyporheic exchanges. These field studies can be used, in some cases, for the calibration of two or three-dimensional numerical groundwater flow models. Conventional methods for quantifying water fluxes across the riverbed include direct measurements from seepage meters (Wroblicky et al., 1998; Duff et al., 2000; Rosenberry et al., 2012) and Darcy flow estimations from pressure head and hydraulic conductivity values collected in piezometers (Anderson et al., 2005). However, these methods present some limitations. Murdoch and Kelly (2003) highlighted the errors induced by resistance in the seepage meter collection system, while Boulton (1993) and Rosenberry and Pitlick (2009) found that coarse sediments and armored layers within the riverbed could represent a problem for the correct placement of the seepage meters. Instead, Surridge et al. (2004) emphasized the difuculties in obtaining reliable hydraulic head and hydraulic conductivity estimates from piezometers.

Innovative methodologies dealt with the use of temperature time series within the river or riverbed to calculate water flow patterns in hyporheic sediments (e.g., Hatch et al., 2006; Keery et al., 2007; Francis et al., 2010; Westhoff et al., 2011; Lautz and Ribaudo, 2012). The main advantages of these techniques are the easier installation of temperature sensors in comparison to that of the piezometers and the lower costs. The use of temperature-based methods in conjunction with Darcy-based methods was also supported by some authors (e.g., Alexander and Caissie, 2003; Krause

et al., 2012; Angermann et al., 2012).

A very common approach implies the implementation of stream transport models with parameters derived from conservative stream tracer experiments. In this approach the hyporheic exchanges are studied from the stream perspective as transient storages of surface waters. These models, referred as phenomenological models, do not have necessarily a physical meaning, because, differently from the physical-based models, they do not focus on the dynamics of the physical processes generating the water storage. Thus,the results obtained for a particular water system cannot be extended to another one with different characteristics. Besides, Harvey and Wagner (2000) argued that tracer experiment results, from which model parameters are derived, are very sensitive to the experimental setup (i.e., the "window of detection"), such as the length of the experimental reach.

Several phenomenological models were proposed by the scientific literature, such as the transient storage model (Bencala and Walters, 1983; Runkel et al., 1998), the STIR model and the continuous time random approach. In transient storage models (TSM) the hyporheic exchange is considered as a diffusive (Marion and Zaramella, 2005; Qian et al., 2008; De Smedt, 2007) or as a first-order mass transfer process (Bencala, 1984; O'Connor, 1988; De Smedt, 2006) between the hyporheic zone and the open stream channel compartments, with an exponential form of the solute Residence Time Distribution (RTD) in hyporheic sediments. TSM models represent simple and practical tools for the estimation of water and solute exchange through the streambed but they also need to be carefully applied due to their limitations (Marion et al., 2003). Zaramella et al. (2003) underlined the limits of TSM application in deep sediment beds, while (Haggerty et al., 2002) studied a power-law residence time distribution and showed that hyporheic zone has a very wide range of timescales. Recently, Zaramella et al. (2003) and Bencala (2005) also focused on the wide variations of time scales associated with the advective transport in the streambed, in contrast to the single rate approximation made in the TSM. Finally, it is important to recall that the presence of vegetation and other in-stream dead zones of recirculating water can induce a transient storage of solutes which is not related to

hyporheic exchange and that is identified by TSM (Salehin et al., 2003).

This limit is partially overcome by the STIR model, which disguishes the different storage processes and, in particular, the fast exchanges, induced by dead zones, from the slow ones, related to hyporheic processes (Marion et al., 2008b). The solute downwstream fluxes are assumed to be controlled by the exchanges with different storage zones, each one characterized by a specific residence time distribution, that can differs from the exponential one. Thus, the STIR model have a good applicability in problems requiring a detailed estimate of hyporheic contamination. Instead, in cases where there is no need to distinguish between the different storage processes less complex models, with fewer parameters, like the TSM, are preferred.

In the continuoos time random walk (CTRW) model the motion of solute particles is considered as a sequence of random jumps of variable lenght and duration (Montroll and Weiss, 1965; Scher and Lax, 1973). The concentration of a solute at a given time and position is statistically derived as the probability for a solute particle to occupy the specific position at the specific time (Boano et al., 2007a).

Physically-based models are based on physical mass and momentum balance equations that link the surface and subsurface pressure variations to the hyporheic transport. The upwelling and downwelling water fluxes, controlled by the pressure variations at the sediment-water interface, are then related to the solute residence times in bed. These models have a lower applicability, in comparison to the TSM, since they require a good knowledge of the main sedimentological and morphological characteristics of the system of interest. However, if these physical properties are available, they can provide a detailed prediction of transport patterns, and they can be used to complement direct observations.

Physically-based models can be divided in two groups, i.e., advective models and advective-dispersive models. The dispersive effect was found negligible for quantifying solute mass exchange with bedforms by Eylers et al. (1995) and Packman et al. (2000). Advective models were also employed by Elliott and Brooks (1997b), Boano et al. (2006a) and similar studies. However, simulations of

both advective and dispersive transport in streambeds were performed by Cardenas et al. (2008b), Bottacin-Busolin and Marion (2010) and Sawyer and Cardenas (2009). Besides, Jin et al. (2010) demonstrated with laboratory experiments and numerical simulations that both advective and dispersive transport components play an essential role for hyporheic exchange processes and that advective models underestimate the rate and total mass of solute transfer.

1.2.1 Reach-scale fluxes

The hyporheic exchange at reach scale is primarily driven by topography and changes in bed permeability. Horizontal hyporheic exchange also occurs, due to the presence of alternate bars and large meander point bars or channel sinuosity. Alternate bars represent the predominant geomorphological feature in low-curvature channels. Instead, high-curvature channels are usually characterized by large meander point bars at the inner bank of channel beds, caused by erosion and sedimentation processes.
Several researchers studied the influence of large-scale features on hyporheic exchange with field studies (Harvey and Wagner, 2000; Wondzell, 2006) or numerical simulations (Saenger et al., 2005; Gooseff et al., 2006). Recently, Marzadri et al. (2010) investigated the effects of an alternate bar morphology in gravel bed rivers and they found a dependence of the mean value and the variance of the hyporheic residence time on the alternate bar amplitude at equilibrium.

River sinuosity also proved to induce the formation of complex patterns of water exchange at the scale of the meander wavelenght scale (Poole et al., 2006; Zarnetske et al., 2008). Boano et al. (2010) defined a characteristic spatial pattern of hyporheic exchange in meandering streams, dependent on the stream curvature, with water upwelling and downwelling concentrated near the stream banks. Revelli et al. (2008) and Cardenas (2008a) demonstrated that hyporheic fluxes in the lateral intrameander floodplain are driven by differences in stream surface elevation along the river and are characterized by longer residence times in comparison to those due to bedforms or bars.

17

1.2.2 Bedform-scale fluxes

The hyporheic exchange at bedform scale is mainly caused by the presence of morphological features such as dunes, ripples, anti-dunes and obstacles (e.g., logs, boulders, beaver dams, weirs).

Elliott and Brooks (1997a,b) proposed and calibrated (trough laboratory flume experiments) a semi-analytical description of the flow field and the solute residence time distribution in a stream-bed characaterized by bedforms. In particular they highlighted the importance of two mechanisms of "pumping" and "turnover" for water transport in the sediments. The former, observed by Savant et al. (1987), is due to the acceleration of streamflow over the bedforms and the separation of the flow at the crest, that induce pressure variations at the bed surface and, consequently, flow into and out of the sediments (water enters the streambed on the bed-form stoss face and leaves the sediments on the lee face). The latter is caused by the continuous trapping and release of pore water during bedform movement, in turn due to erosion/sedimentation processes. Elliott and Brooks (1997b) estimated the bedform-induced hyporheic exchange by applying a sinusoidal head distribution on a flat surface, that represented the top boundary of the bed (Figure 1.6). This approach was further recalled in other studies (e.g., Bottacin-Busolin and Marion, 2010; Jin et al., 2010).

Numerical simulations with periodic triangular bedforms were performed by Packman and Brooks (2001) and Cardenas and Wilson (2007b) in order to study the pore water circulation in the streambed generated by current-bedform interactions, with under-flow in the deeper part. Marion et al. (2002) investigated the effect of bedform geometry on solute penetration depth in the sediments and they found that subsurface flow is affected both by the amplitude and the wavelenght of bedforms. Cardenas and Wilson (2007c) estimated water penetration depths in the streambed of between 60 and 80% of bedform wavelengths. Other studies examined the effect of arbitrary surface topography (Wörman et al., 2007), unsteady flows (Boano et al., 2006b) and groundwater discharge (Boano et al., 2008) on bedform-induced hyporheic fluxes.

The impact of heterogeneities of streambed hydraulic properties was also investigated (Salehin et al., 2004; Marion et al., 2008a; Sawyer and Cardenas, 2009). For instance, Cardenas et al. (2004)
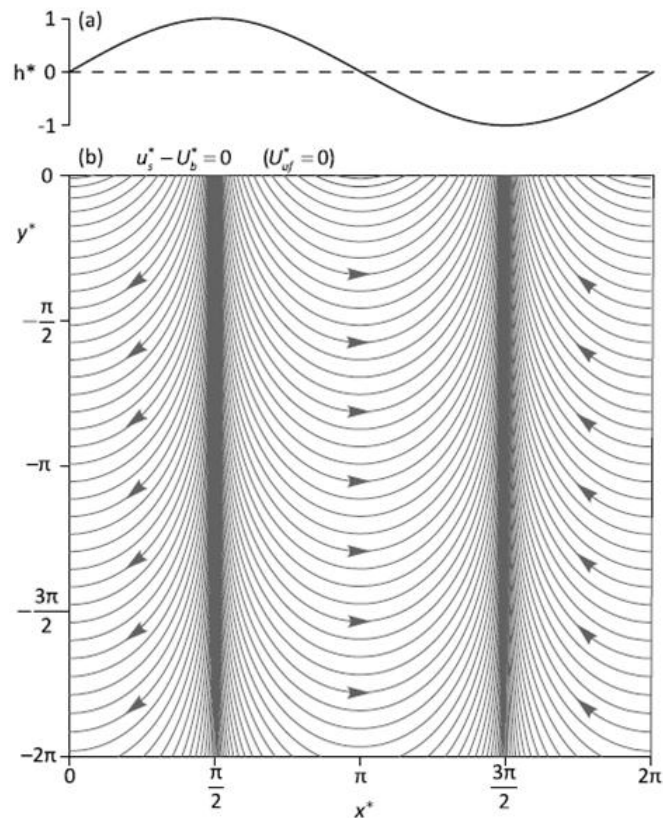
Figure 1.6: Bedform-induced sinusoidal head distribution adopted by Elliott and Brooks (1997b) (from Bottacin-Busolin and Marion, 2010).

identified additional significant hyporheic fluxes caused by sediment heterogeneity while Salehin et al. (2004) found more spatially limited hyporheic exchanges and higher water fluxes in heterogeneous sediments than in homogeneous ones. However, Sawyer and Cardenas (2009) also reported cases where the heterogeneity effect on flow paths do not correspond to a significant change in RTD.

19

1.3   Reactive solute dynamics

The hyporheic zone has a high potential of stream solute attenuation and removal. In fact, rich microbial and invertebrate communities, associated to steep chemical gradients and dynamic exchanges of oxygen, carbon and nutrients, result in more intense and rapid biogeochemical processes than in aquifer sediments or stream water (Naegeli and Uehlinger, 1997; Fischer and Pusch, 2001). Solutes entering the sediments with water can be transformed into reduced or oxidized substances through reactions mediated by hyporheic bacteria before coming back to the stream. Other attenuation processes also occur, such as sorption to mineral surfaces and organic carbon and precipitation. These non-destructive processes are important for the retardation of transport of metals and other non-degradable substances. For example, Gandy et al. (2007) demonstrated the role of attenuation of mining-derived pollutants by the hyporheic zones. The most favourable removal zones were those enhancing precipitation/adsorption of dissolved minerals and reactions. However, despite these mechanisms retard solute movement in the sediments and reduce pore water solute concentrations, they do not alter the total solute mass in the whole environmental system.

Several studies also focused on hyporheic removal of nutrients (e.g., nitrate and posphate) by biologically mediated redox reactions or secondary reactions. Lautz and Fanelli (2008) and Krause et al. (2009) investigated the complex patterns of nitrate attenuation and production at small scales. In fact, nitrate on the one hand can be removed by denitrification but on the other hand can be produced by nitrification. The competition between these reactions defines the net nitrate removal or production in the hyporheic zone. The efficiency of these hyporheic reactions depends on redox conditions and DOC availability but also on solute residence times in the hyporheic zone. Pinay et al. (2009) found that the influence of biological processes on nitrate fluxes was function of the interplay between residence times and reaction rates.

The interaction of hydrology and biogeochemistry in the hyporheic zone was taken into account in different studies of fluvial environments (e.g., Gu et al., 2007; O'Connor and Hondzo, 2008). In particular, Harvey and Fuller (1998) and Fuller and Harvey

(2000) provided observations of solute concentration gradients and reaction rates beneath stream bedforms, and underlined the role of the hyporheic zone in enhancing microbially mediated processes. Recently, mathematical models have been increasingly used to investigate the effect of coupled hydrological and biogeochemical processes on the fate of nutrients. For instance, Cardenas et al. (2008a) provided a model for a rippled permeable seabed, by sequentially modeling turbulent-oscillatory flow, flow in the porous medium, and biogeochemical reactions. Another modeling approach was developed by Boano et al. (2010), who investigated the biogeochemical patterns and the temporal evolution of reactive solutes in the hyporheic region of a meandering river, by estimating and comparing the typical kinematic and chemical timescales (Figure 1.7). Marzadri et al. (2012) studied the influence of stream morphology, water temperature and nutrient concentrations on nitrate removal potential by applying a multi reactive advection-dispersion equation to an alternate-bar morphology. However, we are far for a complete understanding of the complex links between the hydrodynamical and biogeochemical processes in the hyporheic zone (Fleckenstein et al., 2010).
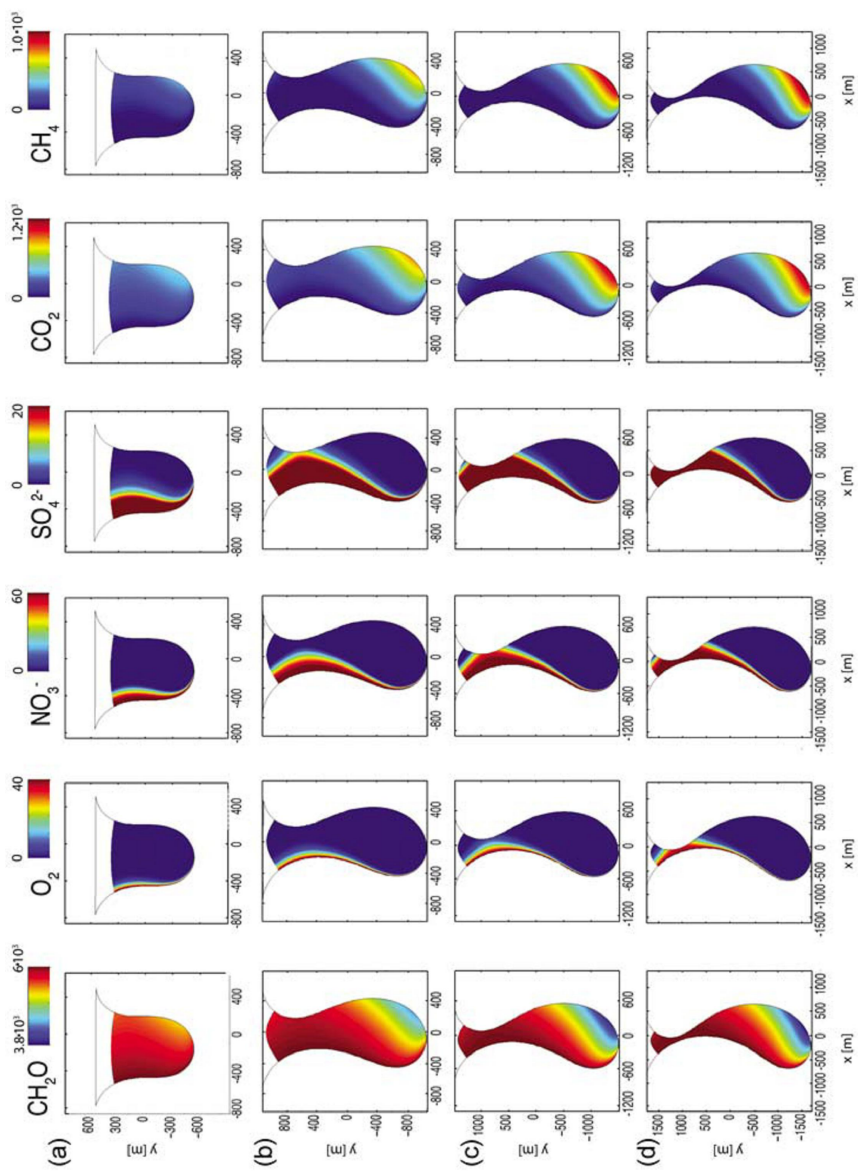
Figure 1.7: Steady-state solute concentrations for different stages of meander evolution (from Boano et al., 2010).
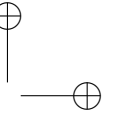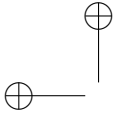
Chapter 2

Chemical zonation in dune-induced hyporheic zones

2.1 Introduction

Water and solute exchange across the riverbed plays a fundamental role in the ecology and quality of fluvial environments (Findlay, 1995; Alexander et al., 2000; Battin et al., 2008; Bottacin-Busolin et al., 2009). The stream-borne chemicals entering the hyporheic zone are subject to biogeochemical transformation before returning to the river, and their fate is controlled by the interplay of both hydrological and biochemical processes (Smith et al., 2008). For this reason a good knowledge of hyporheic exchange processes is essential for the assessment of chemical zonation and nutrient transformation in the fluvial environment.

In this chapter we will investigate the influence of surface water-groundwater exchange on the main microbial transformations of nutrients occurring in the hyporheic zone. In particular, we will develop a numerical model to analyze the exchange triggered by a duned streambed, that represents a widespread configuration in fluvial environments. Our aim is to shed light on the effects of this kind of bed forms on transport and reaction processes of organic carbon and nitrogen, in order to provide significant insights for stream biogeochemistry.
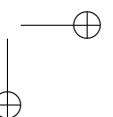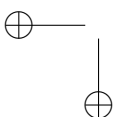
The main results will be the description of the steady-state spatial distribution of water-borne solutes below a stream dune and the analysis of the effects of stream water quality, stream velocity, and sediment permeability on the reaction patterns. We will consider four representative reactive compounds: dissolved organic carbon (DOC), oxygen (O_2), nitrate (NO_3^-) and ammonium (NH_4^+). We choose these chemicals because they are usually used as indicators of water quality in field studies (Aitkenhead-Peterson et al., 2009) and they have a direct influence on the processes in the river ecosystem.

2.2 Model description

The problem of interest is sketched in Figure 2.1. We consider a stream with mean water depth, *d*, and bulk velocity, *U*. The streambed is formed of two-dimensional periodic dunes, triangular in shape, with height *H* and length *L*. The dunes are asymmetric because of the constant direction of the stream flow, and the position of the crest (L_c) is shifted towards the downstream end of the dune. A Cartesian reference system is adopted, with *x* and *y* as the streamwise and upward coordinates, respectively, and the axis origin is placed at the dune trough. Due to the periodicity of the streambed in the streamwise direction, we focus on a single-dune cell of the 2D domain.

The goal is to estimate the spatial distribution of four solutes under the bed forms in steady-state conditions, given the physical and chemical properties of the stream and the hydraulic properties of the sediments. The compounds of interest are DOC, oxygen, nitrate and ammonium. We choose formaldehyde (CH_2O) to represent the DOC substance for its simple chemical structure and because it can be a degradation product of more complicated DOC compounds. Moreover, it is usually selected as the representative DOC compound for numerical simulations or field investigations (e.g., Hunter et al., 1998).

Firstly, turbulent flow in the stream will be simulated and values of pressure on the streambed will be evaluated. Then, we the solute concentrations below the dune surface will be numerically simulated, by considering both the advective and dispersive flows
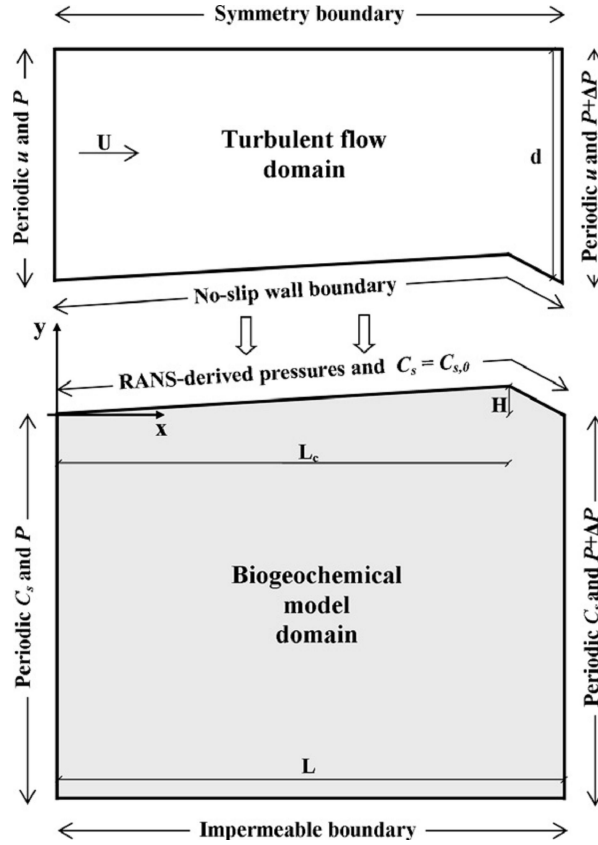
Figure 2.1: Modeling scheme. Top part shows the pressure and velocity boundary conditions for the stream water turbulent flow over the streambed; bottom part shows the pressure and concentration boundary conditions for the solute reactive transport in the porous medium. The model domain represents an asymmetrical stream dune of length $L = 1$ m, height $H = 0.075$ m, with the crest shifted on the right ($L_c = 0.9$ m). The streambed depth is 0.8 m. The stream velocity U varies from 0.21 to 0.39 m/s in the simulations.

and the biochemical processes. The governing equations of the pressure distribution, the hyporheic flow field and the biogeochemical reactions are described in the next sections.

25

2.2.1 Pressure Distribution

The turbulent water flow over the dunes is simulated by numerically solving, in steady-state conditions, a finite-volume formulation of the Reynolds-Averaged Navier-Stokes (RANS) equations for an incompressible, homogeneous fluid (Cardenas and Wilson, 2007b)

$$\frac{\partial U_i}{\partial x_i} = 0 \tag{2.1}$$

$$\rho U_j \frac{\partial U_i}{\partial x_j} = -\frac{\partial P}{\partial x_i} + \frac{\partial}{\partial x_j}\left(2\mu S_{ij} - \rho \overline{u_j' u_i'}\right) \tag{2.2}$$

where $i, j = 1, 2$ are spatial indexes corresponding to x and y directions ($x_1 = x$, $x_2 = y$), ρ and μ are water density and dynamic viscosity, respectively, t is time, U_i and u_i' are the time-averaged and turbulent velocity components in x_i direction, respectively, and P is time-averaged pressure. $S_{i,j}$ is the strain rate tensor

$$S_{i,j} = \frac{1}{2}\left(\frac{\partial U_i}{\partial x_j} + \frac{\partial U_j}{\partial x_i}\right), \tag{2.3}$$

while $-\overline{u_j' u_i'} = \tau_{ij}/\rho$ is the mean strain rate related to the Reynolds stresses (τ_{ij}) by

$$-\overline{u_j' u_i'} = \nu_t \left(2S_{ij}\right) - \frac{2}{3}\delta_{ij}k \tag{2.4}$$

where ν_t is the kinematic eddy viscosity, δ_{ij} is the Kronecker delta, and k is the turbulent kinetic energy.

The evaluation of the turbulent strain rates requires the adoption of a closure scheme to determine the eddy viscosity ν_t. Here, the $k - \omega$ turbulence closure scheme (Wilcox, 1991) is adopted, with the eddy viscosity

$$\nu_t = \frac{k}{\omega}, \tag{2.5}$$

the specific dissipation ω,

$$\omega = \frac{\epsilon}{\beta^* k} \tag{2.6}$$

the turbulence dissipation rate ϵ, and the closure coefficient β^*. Two additional equations for k and ω are required to complete the

closure scheme. The steady state transport equations for k and ω are

$$\rho \frac{\partial (U_j k)}{\partial x_j} = \rho \tau_{ij} \frac{\partial U_i}{\partial x_j} - \beta^* \rho \omega k + \frac{\partial}{\partial x_j} \left[(\mu + \mu_t \sigma_k) \frac{\partial k}{\partial x_j} \right] \qquad (2.7)$$

$$\rho \frac{\partial (U_j \omega)}{\partial x_j} = \alpha \frac{\rho \omega}{k} \tau_{ij} \frac{\partial U_i}{\partial x_j} - \beta \rho \omega^2 k + \frac{\partial}{\partial x_j} \left[(\mu + \mu_t \sigma_\omega) \frac{\partial \omega}{\partial x_j} \right] \quad (2.8)$$

The standard closure coefficient values are $\alpha = 5/9$, $\beta = 3/40$, $\beta^* = 9/100$, and $\sigma_k = \sigma_\omega = 0.5$ (Cardenas and Wilson, 2007b).

The RANS domain is represented by the water column above a single dune (Figure 2.1). A spatially periodic pressure condition is prescribed on the lateral boundaries, with an additional pressure drop ΔP between the left and right domain sides, in order to consider the stream gradient. We assume therefore that the water columns over two subsequent dunes exhibit the same pressure distribution and a constant difference in magnitude, with lower values downstream. The pressure drop is derived from the bed slope i_b and the dune length L by applying the equation $\Delta P = i_b L g \rho$. A symmetry boundary condition (i.e., no fluxes) is set at the top of the RANS domain since water depth is significantly larger than the dune height ($d \ll H$) and the submergence was high. Thus, the free surface is not influenced by the presence of bedforms and it is possible to replace it with the symmetry condition. Finally, no-slip wall boundary conditions ($U_j = 0$) are applied at the bottom of the domain. This allow us to solve the problem for turbulent flow neglecting the influence of the subsurface flow in the sediments on the surface flow, which is a standard assumption since subsurface flow rates are usually much smaller than those in the stream. The RANS simulations are solved using a finite-volume approach with a variable number of grid elements (from 16,000 to more than 80,000) and a denser node spatial distribution near the bottom of the domain. Further details can be found in Cardenas and Wilson (2007b).

From the solution of the RANS model, the pressure distribution on the duned streambed is obtained. Figure 2.2 shows some streambed pressure distributions on a 1-meter-long dune for different values of the Reynolds number $Re = U \cdot d / \nu$, where ν is the

kinematic water viscosity. All pressure profiles have an asymmetrical shape, with a maximum at $x = 0.3$ m and a marked minimum at the dune cres ($x = 0.9$ m). The figure shows that an increase of the stream velocity leads to higher values of surface pressures. The resulting pressure gradients determine the water exchange with the sediments, as described in the next section.
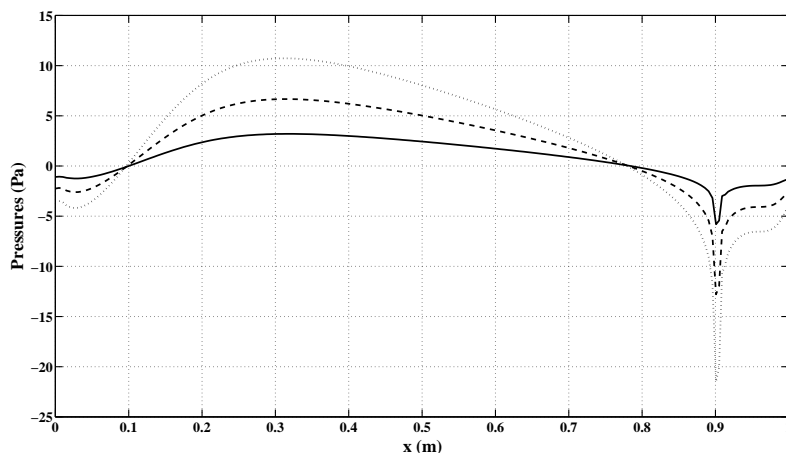
Figure 2.2: RANS-derived pressure distributions for stream velocities $U = 0.21$ m/s (solid line), 0.30 m/s (dashed line) and 0.39 m/s (dotted line), corresponding to Reynolds numbers $Re = 106{,}670$, 154,120 and 195,630, respectively ($L = 1$ m, $L_c = 0.9$ m, $H = 0.075$ m, $d = 0.5$ m).

2.2.2 Hyporheic flow field and biochemical reactions

The pressure distribution over the dune is used as a boundary condition in the multi-component reactive transport model in order to predict the solute fluxes and concentrations in the hyporheic zone, considering both the fluid dynamics and biogeochemical processes. For this purpose, the hyporheic flow modeling represents a key step, since it determines the advective and dispersive transport patterns of the substances in the hyporheic zone.

The advective exchange of water across a duned streambed can be driven by two mechanisms of "pumping" and "turnover": the former is due to the presence of pressure gradients over the bed

forms, the latter is linked to the temporary trapping and release of water by moving bed forms (Elliott and Brooks, 1997b). In our work we assume that the dunes are not moving, since preliminary numerical simulations (not shown) indicated that water fluxes induced by turnover are negligible for our system.

The water flow under the bed surface in steady-state conditions is estimated using the groundwater flow equations, i.e., the Darcy's law and the continuity equation

$$\mathbf{q} = -\frac{\kappa}{\mu} \left(\nabla P + \rho g \nabla y \right) \tag{2.9}$$

$$\nabla^2 \left(\frac{P}{\rho g} + y \right) = 0, \tag{2.10}$$

where $\mathbf{q} = (q_x, q_y)$ is the Darcian velocity vector, κ is the permeability of the porous medium (assumed homogeneous), g is the gravitational acceleration, ρ is the water density, and P is the water pressure in the porous medium. The velocity $\mathbf{q}$ includes both the pumping-induced flow and the basic groundwater flow, the latter due to the stream gradient. The pressure boundary conditions are described later.

As to the biochemical processes, the model considers three reactions, mediated by subsurface microorganisms: aerobic respiration, denitrification and nitrification (see Table 2.1). Reactions r_1 and r_2 describe the heterotrophic DOC biodegradation, with the DOC as the electron donor and the oxygen (aerobic respiration) and nitrate (denitrification) as the electron acceptors, respectively. Reaction r_3 represents nitrification, i.e., the biological autotrophic oxidation of ammonium into nitrate, with oxygen as electron acceptor. Aerobic respiration and nitrification start simultaneously, while denitrification only occurs when oxygen concentration falls under a limiting value, i.e., when anaerobic conditions are established.

29

Table 2.1: List of the reactions considered in the simulations.

Reaction index	Reaction type	Reaction	β_i value
r_1	Aerobic respiration	$CH_2O + O_2 \longrightarrow CO_2 + H_2O$	1
r_2	Denitrification	$5CH_2O + 4NO_3^- + 4H^+ \longrightarrow 5CO_2 + 2N_2 + 7H_2O$	0.8
r_3	Nitrification	$NH_4^+ + 2O_2 \rightarrow NO_3^- + 2H^+ + H_2O$	-

For the definition of the reaction kinetics we follow the approach described by Hunter et al. (1998) and, for redox reactions r_1 and r_2, we consider separetely the rate of DOC oxidation and the rate of the i-th reduction half-reaction.

First-order degradation kinetics is assumed for the DOC oxidation rate Γ_{DOC}

$$\Gamma_{DOC} = k_{DOC} \cdot C_{DOC} \tag{2.11}$$

where k_{DOC} is the DOC decay constant and C_{DOC} is the DOC molar concentration. The linear kinetics in Equation (2.11) is the simplest way to model DOC degradation, but it could be replaced by more complex formulations (e.g., Monod) at the expense of a higher number of parameters.

The rate of reduction $\Gamma_{red,i}$ of the i-th electron acceptor ($i = 1$ for oxygen, $i= 2$ for nitrate) is estimated by

$$\Gamma_{red,i} = \beta_i \cdot \Gamma_{DOC} \cdot f_i \qquad i = 1,2 \tag{2.12}$$

where $\boldsymbol{\beta_i}$ represents the ratio between the moles of transferred electrons per mole of oxidized DOC and the moles of electrons per mole of reduced compound in the i-th reaction, and f_i is the fraction of electrons consumed by the i-th reduction half-reaction. Values of β_i are given in Table 2.1. The f_i parameter is evaluated with a simplified Monod formulation

$$f_i = \left(1 - \sum_{n=0}^{i-1} f_n \right) \cdot \alpha_i \tag{2.13}$$

with $f_0 = 0$ and

$$\alpha_i = \begin{cases} \frac{C_i}{C_{i,lim}} & \text{if } C_i < C_{i,lim} \\ 1 & \text{if } C_i \geq C_{i,lim} \end{cases}. \tag{2.14}$$

α_i is a dimensionless parameter that considers the limitation of $\Gamma_{red,i}$ due to the availability of the i-th reaction electron acceptor, while C_i and $C_{i,lim}$ are, respectively, the molar concentration and the molar limiting concentration of the i-th reaction electron acceptor. When the electron acceptor exceeds the limiting concentration, the reduction rate is independent of C_i, while in the case of lower concentrations $\Gamma_{red,i}$ is linearly proportional to C_i.

31

Lastly, a bimolecular expression is used for the nitrification (r_3) rate Γ_{nitr}

$$\Gamma_{nitr} = k_n \cdot C_{NH_4^+} \cdot C_{O_2} \tag{2.15}$$

where k_n is the second-order nitrification molar rate coefficient, $C_{NH_4^+}$ and C_{O_2} are the molar concentrations of ammonium and oxygen, respectively. Since the aim of the present work is to study the reactive behavior of hyporheic sediments in response to stream water quality and velocity and to sediment properties, we neglect the influence of temperature on reaction kinetics.

From Equations (2.11)–(2.15) we define the net production rates of the four compounds of interest, adopting a negative sign for reaction terms decreasing the solute concentration

$$\frac{\mathrm{d}C_{DOC}}{\mathrm{d}t} = -\Gamma_{DOC} \equiv R_{DOC} \tag{2.16}$$

$$\frac{\mathrm{d}C_{O_2}}{\mathrm{d}t} = -\Gamma_{red,1} - 2\Gamma_{nitr} \equiv R_{O_2} \tag{2.17}$$

$$\frac{\mathrm{d}C_{NO_3^-}}{\mathrm{d}t} = -\Gamma_{red,2} + \Gamma_{nitr} \equiv R_{NO_3^-} \tag{2.18}$$

$$\frac{\mathrm{d}C_{NH_4^+}}{\mathrm{d}t} = -\Gamma_{nitr} \equiv R_{NH_4^+} \tag{2.19}$$

DOC and ammonium show a negative one-term equation (Equations (2.16) and (2.19)), since they take part as reactants in one process, DOC oxidation half-reaction and nitrification, respectively. Instead, oxygen and nitrate display double-term expressions (Equations (2.17) and (2.18)), with different signs because they act, with different roles, in two reactions. The oxygen is consumed by both aerobic respiration r_1 and nitrification r_3, while nitrate is removed by denitrification r_2 and produced by nitrification r_3. The contribution of the different terms varies in time, according to the reactant concentrations.

The overall reaction rates (Equations (2.16)–(2.19)) are then coupled with the hyporheic flow field (obtained by Equations (2.9) and (2.10)) and hydrodynamic dispersion in order to define the governing equations of the steady-state reactive solute transport model

$$\theta R_s = \nabla(-\theta \mathbf{D} \nabla C_s + \mathbf{q} \cdot C_s) \qquad s = \mathrm{DOC, O_2, NO_3^-, NH_4^+} \tag{2.20}$$

32

where θ is the sediment porosity, R_s is the consumption / production rate of the compound s, $\mathbf{D}$ is the hydrodynamic dispersion tensor and C_s is the molar concentration of the chemical s. The expressions (2.20) are valid in steady-state conditions and under the assumptions of no sorption phenomena and no solute source in the porous medium. The influence of pH variation on reaction kinetics is also considered negligible, due to the buffering capacity of other chemical processes occurring in the hyporheic zone. Dispersion represents a solute transport process, additional to the advective one, contributing to the spreading of the chemicals in the hyporheic zone. In particular, hydrodynamic dispersion combines mechanical dispersion, induced by the local velocity variations, and molecular diffusion, caused by concentration gradients at microscopic level. The elements of the dispersion tensor are (Bear and Verruijt, 1992)

$$\theta D_{ij} = (\alpha_L - \alpha_T) \cdot \frac{q_i q_j}{|\mathbf{q}|} + \delta_{ij} \cdot (\alpha_T |\mathbf{q}| + \theta \cdot \tau D_{mol}) \qquad (2.21)$$

where i, j = 1, 2, α_L and α_T are the longitudinal and transversal dispersivities, respectively, τ is the tortuosity factor, and D_{mol} is the molecular diffusion coefficient. The values of the dispersivities α_L and α_T depend on sediment size and heterogeneity of the porous medium.

The biogeochemical model domain is a single dune, triangular in shape (see Figure 2.1). As to the boundary conditions, we impose on the lateral boundaries the periodic conditions

$$P(x_{min}, y) = P(x_{max}, y) + \Delta P \qquad (2.22)$$

$$C_s(x_{min}, y) = C_s(x_{max}, y) \qquad (2.23)$$

with x_{min} and x_{max} as the horizontal coordinates of the initial and terminal points of the dune and ΔP as the pressure drop between the lateral boundaries of the domain, equal to that one applied to the free surface.

On the upper layer, i.e., on the sediment-water interface, we prescribe a Dirichlet condition with the RANS-derived pressure distribution and the constant solute concentrations in the stream. Finally, a no flow condition is applied to all the substances at the bottom of the dune, and the porous media is chosen deep enough so as not to affect the pathlines in the main zone of study, close to the bed surface.

2.3 Results

The chemical zonation in the streambed is investigated through the numerical simulation of the governing equations of the reactive solute transport model. For this purpose, we employ Comsol Multiphysics, a numerical software that uses a finite-volume approach, with adaptive meshing and error control. In particular, we choose a non uniform mesh, with a higher node density in the zone of interest, near the bed surface, for a total number of 3,781 grid nodes and 7,216 triangular elements.

We consider a typical dune triangular geometry, with a length $L = 1$ m, a bed form height $H = 0.075$ m and the crest located at $L_c = 0.9$ m (asymmetric dune, see Figure 2.1). The streambed is homogeneous and isotropic, with a porosity $\theta = 0.4$ and a tortuosity factor $\tau = 0.74$, while the mean water depth, d, is 0.5 m. With regard to the reaction constants, we choose values within the ranges suggested by VanCappellen and Wang (1996). In order to consider a typical average condition, for the nitrification rate constant we use the value $k_n = 5 \cdot 10^{-6}$ L/(mg s), while for the DOC reaction rate we select $k_{DOC} = 5 \cdot 10^{-6}$ s^{-1}. Oxygen and nitrate limiting concentrations ($C_{O_2,lim}$ and $C_{NO_3^-,lim}$) are set at 1 mg/L and 0.5 mg/L, respectively. As to the other physical and chemical parameters, i.e., the in-stream solute concentrations, the stream velocity U, the sediment permeability κ and dispersivities α_L and α_T, we perform a sensitivity analysis in order to investigate their impact on the biogeochemical processes in the streambed.

2.3.1 Impact of stream water quality

Three configurations, characterized by different values of in-stream solute concentrations (see Table 2.2), are considered: a strongly polluted stream (case 1), with high nutrient concentrations (like those described by Aitkenhead-Peterson et al., 2009), a pristine stream with no DOC limitation (case 2) and a pristine stream with DOC limitation (case 3). The pristine stream configuration is split in two cases in order to consider the remarkable effects of DOC availability on the kinetics of reactions. The permeability κ is set equal to 10^{-10} m^2, characteristic of well-sorted coarse sands to

Table 2.2: Solute in-stream concentrations for cases 1, 2 and 3.

Case	$C_{\text{DOC},0}$ mg/L	$C_{\text{O}_2,0}$ mg/L	$C_{\text{NO}_3^-,0}$ mg/L	$C_{\text{NH}_4^+,0}$ mg/L
1	150	10	8	5.00
2	50.0	10	1	0.05
3	5.00	10	1	0.05

gravels. The longitudinal dispersivity is assumed equal to 3 mm (i.e., a few grain diameters), while the transversal dispersivity α_T is a tenth of the longitudinal one α_L. The stream velocity U is 0.34 m/s and the stream slope is $1.5 \cdot 10^{-4}$.

The results of the simulations are displayed in Figures 2.3 (case 1), 2.4 (case 2) and 2.5 (case 3). Two advective flow cells are visible below the streambed surface, with different width and depth. The cell in the right-hand part of the dune is wide and quite deep (65 cm); mean flow direction in the cell is the same as the stream flow. On the contrary, the left cell is narrower and shallower, with mean flow opposite to the stream flow. A stagnation point is also present at the deepest point of this cell. Both advective cells delimit an advective water exchange area, where water from the stream moves along advective flowpaths before leaving the sediments, with different residence times depending on path length. Beneath this zone the flow field is dominated by groundwater underflow, induced by the stream slope, and water flow is not affected by the presence of the dunes. The same reversed hyporheic circulation cells and flow stagnation zones have been recently observed in a flume and modeled by CFD from Endreny et al. (2011). The flow cells have a direct influence on solute spatial distribution. In fact, even though dispersion tends to smooth concentration gradients, the solute concentration fronts clearly reflect the shape of the water exchange area.

The substantial role played by advection and dispersion fluxes is demonstrated in Figure 2.6, where oxygen concentrations of case 2 are shown for different dune vertical sections, in the case of diffusive transport only, i.e., switching off water flow and the resulting
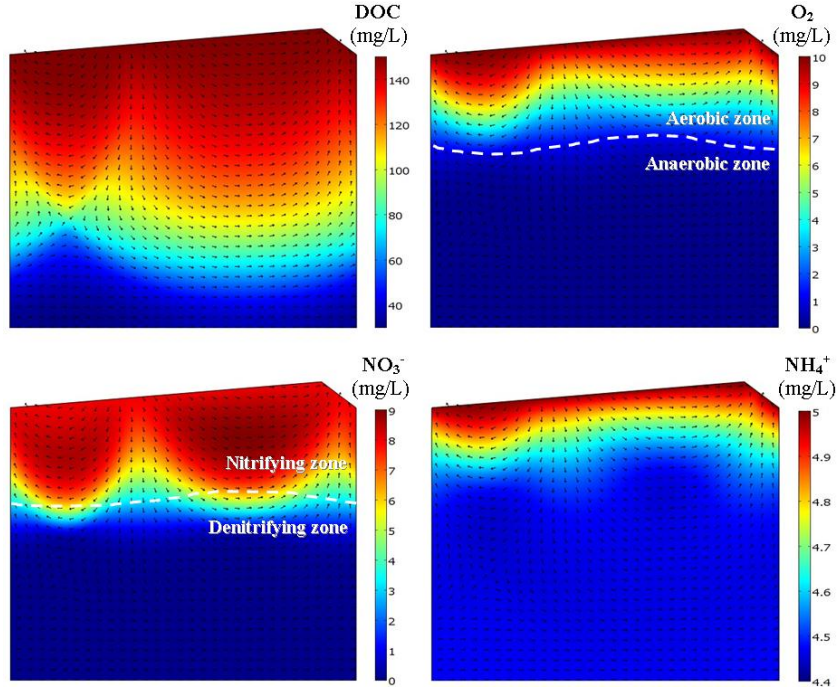
Figure 2.3: Solute spatial distribution for the polluted stream (case 1). Stream velocity is $U = 0.33$ m/s, sediment permeability is $\kappa = 10^{-10} \text{m}^2$, longitudinal dispersivity is $\alpha_L = 3$ mm. DOC reaction rate is $k_{DOC} = 5 \cdot 10^{-6} \text{s}^{-1}$, nitrification rate is $k_n = 5 \cdot 10^{-6}$ L/(mg ·s). In-stream concentrations are shown in Table 2.2. Vectors are only indicative of flow direction.

advective and dispersive fluxes. Oxygen penetration in the porous medium occurs with such a low velocity that the compound is completely removed within the first 5 millimeters of sediments in all the considered sections. Another key point is that the diffusive transport is downward directed, so all solutes entering the sediments are slowly moved to deeper layers and are not returned back to the stream. Thus, the advective and dispersive fluxes are fundamental for controlling the nutrient fate in the streambeds.

We now analyze the three basic cases to investigate the effect of stream water quality. We consider at first the polluted stream configuration shown in Figure 2.3. DOC exhibits a smooth spatial
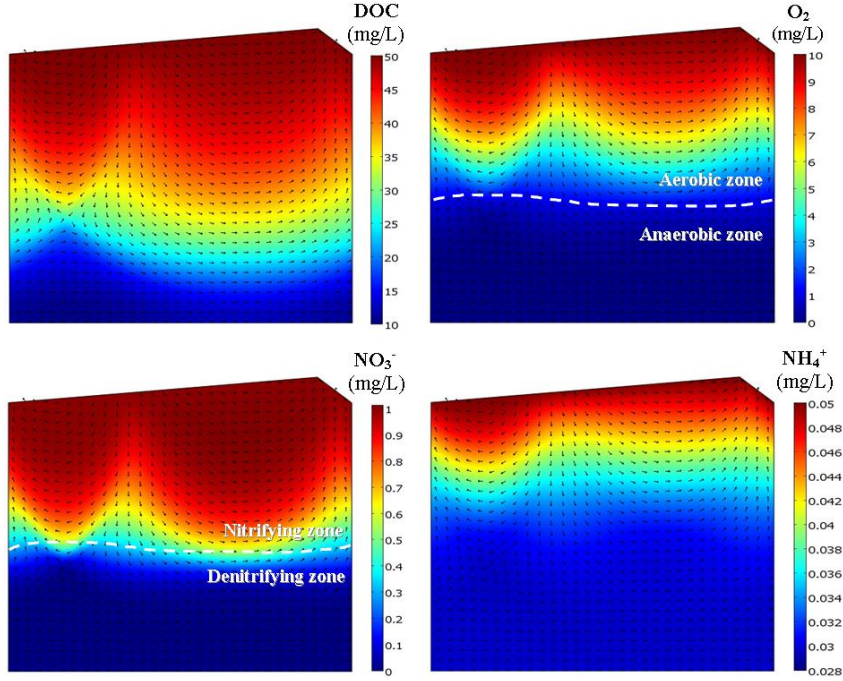
Figure 2.4: Solute spatial distribution for the pristine stream with no DOC limitation (case 2). Stream velocity is $U = 0.33$ m/s, sediment permeability is $\kappa = 10^{-10}$m^2, longitudinal dispersivity is $\alpha_L = 3$ mm. DOC reaction rate is $k_{DOC} = 5 \cdot 10^{-6}$s^{-1}, nitrification rate is $k_n = 5 \cdot 10^{-6}$ L/(mg $\cdot$s). In-stream concentrations are shown in Table 2.2. Vectors are indicative of flow direction.

distribution, with two roughly circular fronts of different sizes and concentrations decreasing with depth. In fact, both advection and dispersion are important mechanisms for delivery of DOC into the porous medium, where it is progressively degraded (Eq. (2.16)). Thus, the hyporheic zone acts as a sink of DOC for the stream. However, the DOC is still present at the bottom of the dune with a concentration of 30 mg/L, since it is not a limiting reactant for the two reactions.

Oxygen displays a similar behavior, with concentration decreasing with depth. However, oxygen fronts are steeper than DOC ones, because of the fast oxygen consumption by two contemporary reactions , i.e., aerobic respiration and nitrification (Equation (2.17)).
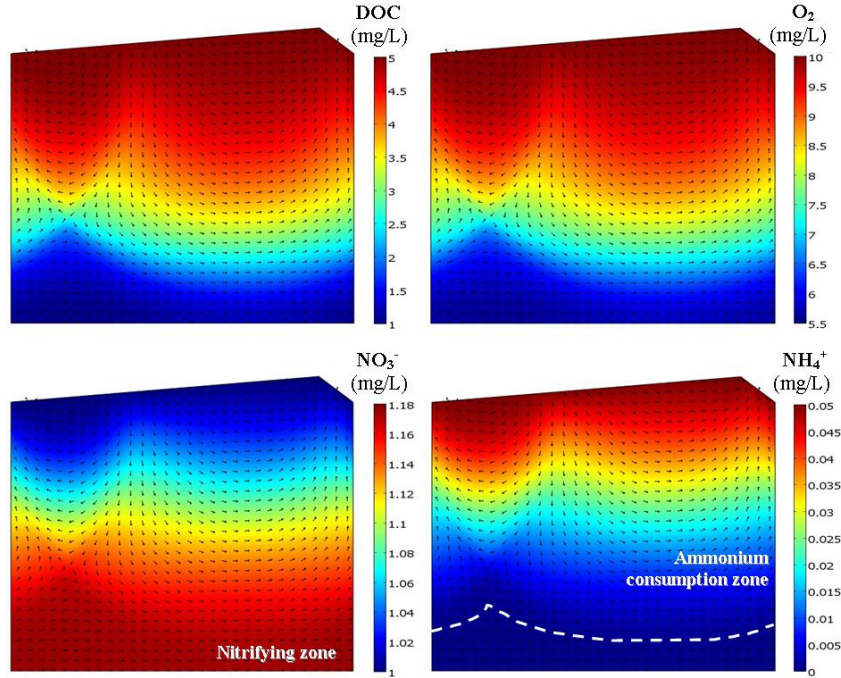
Figure 2.5: Solute spatial distribution for the pristine stream with DOC limitation (case 3). Stream velocity is $U = 0.33$ m/s, sediment permeability is $\kappa = 10^{-10}$m^2, longitudinal dispersivity is α_L = 3 mm. DOC reaction rate is $k_{DOC} = 5 \cdot 10^{-6}$s^{-1}, nitrification rate is $k_n = 5 \cdot 10^{-6}$ L/(mg $\cdot$s). In-stream concentrations are shown in Table 2.2. Vectors are only indicative of flow direction.

Moreover, due to the low in-stream oxygen concentration and the high availability of DOC and NH$_4^+$, oxygen is completely removed within the first 30 cm of depth, i.e. within the water exchange area. These simulated oxygen distributions reproduce well the general features of the patterns observed experimentally by Precht et al. (2004).

Ammonium also exhibits steep fronts and remarkable variations of concentration in the hyporheic zone, because of the fast kinetics of the nitrification process in which it plays the part of the reactant (Equation (2.19)). Eventually, a concentration of 4.5 mg/L is achieved when nitrification stops due to the lack of oxygen. Thus, ammonium spatial distribution is strictly related to the
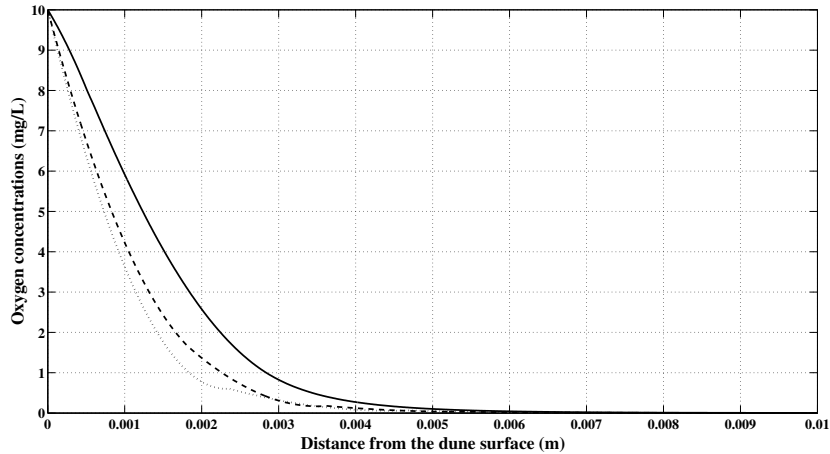
Figure 2.6: Oxygen concentrations for case 2, under diffusive conditions, at x = 0 m (solid line), x = 0.5 m (dashed line) and x = 0.9 m (dotted line).

oxygen zonation.

A different behavior is shown by nitrate, which exhibits a maximum concentration at 15 cm of depth (see Figure 2.3). The reason for this behavior is that the compound has the double role of product and reactant in the nitrification and denitrification reactions, respectively (Equation (2.18)). The removal of nitrate through denitrification begins only when the oxygen falls below the limiting concentration $C_{O_2,lim}$, so up to that threshold the compound is only produced by nitrification. In deeper sediments, denitrification prevails and nitrate is completely removed within the first 35 cm of depth. This behavior is confirmed by Figures 2.7a and 2.7b, that show the spatial patterns of nitrification and denitrification rates. Nitrification rate has a maximum value ($0.34 \text{ mg}/(\text{m}^3 \cdots)$) near the streambed, due to the high concentrations of oxygen and ammonium, and it decreases with depth, as the consequence of the lower reactant concentrations. Instead, denitrification rate displays a downward increase, together with the nitrate concentrations, a maximum value ($0.38 \text{ mg}/(\text{m}^3 \cdots)$) at approximately 35 cm of depth and a fast decrease. Both reactions are active in the
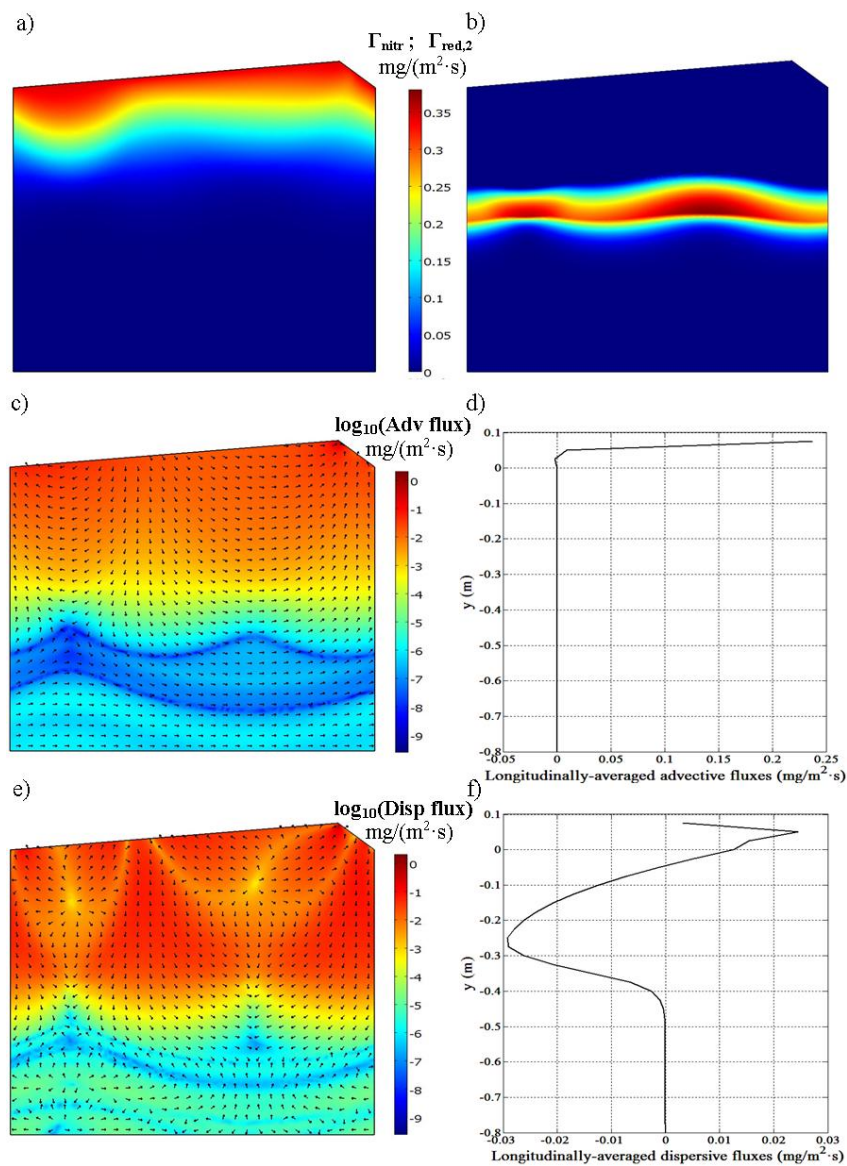
39

Figure 2.7: Nitrification and denitrification rates (Figurese 7a, 7b), logarithmic values and longitudinally-averaged vertical profiles of advective (Figures 7c, 7d) and dispersive (Figures 7e, 7f) fluxes of nitrate (case 1). Vectors are only indicative of flux direction.

central part of the domain, with different rates; as long as nitrification prevails on denitrification there is a net nitrate production and viceversa. The strong nitrate production within the first 20 cm of depth contributes to enhance the nitrate concentration gradient and, consequently, the upward dispersive fluxes (see Equation (2.20)), that are comparable or higher than the advective ones, with the exception of the dune crest (see Figures 2.7c, 2.7d, 2.7e, 2.7f). Part of produced nitrate is released into the stream due to the combination of strong upward advective and dispersive transport, and the dune thus represents a source of nitrate for the stream.

We focus now on the pristine stream configuration with no DOC limitation (case 2, Figure 2.4). All solute in-stream concentrations are lower than in the polluted case, with the exception of oxygen, which keeps the same value (Table 2.2). The decrease of the solute concentrations has a direct influence on the rate of the three studied reactions. Oxygen shows a more gradual decay and wider concentration fronts, due to the decrease of both aerobic respiration and nitrification rates caused by lower concentrations of DOC and ammonium, respectively. The slower oxygen consumption leads in turn to a downward shift of the net denitrifying zone. Thus, nitrate and oxygen are completely removed deeper in the porous medium than in case 1. The spatial patterns of nitrification and denitrification rates are shown in Figures 2.8a and 2.8b. The values are in general one or two orders of magnitude lower than those seen for case 1. Besides, the maximum nitrification rate is highly lower than the denitrification one. The lower nitrate production has a direct effect on the magnitude of the dispersive transport of nitrate. Figures 2.8c, 2.8d, 2.8e and 2.8f show the advective and dispersive fluxes with the former prevalent on the latter in the shallow layers. In this case the dune represents a sink of nitrate for the stream.

The wider concentration fronts are even more evident for the pristine stream configuration with DOC limitation (case 3, Figure 2.5). Aerobic respiration rate is so slow, due to the DOC scarcity, that oxygen can be found even at the bottom of the streambed (6 mg/L), preventing the denitrification process which requires anaerobic conditions. Thus, denitrification does not occur in the sediments in this case. Aerobic respiration is active up to the bottom of the streambed, while nitrification stops shallower, at 60 cm of
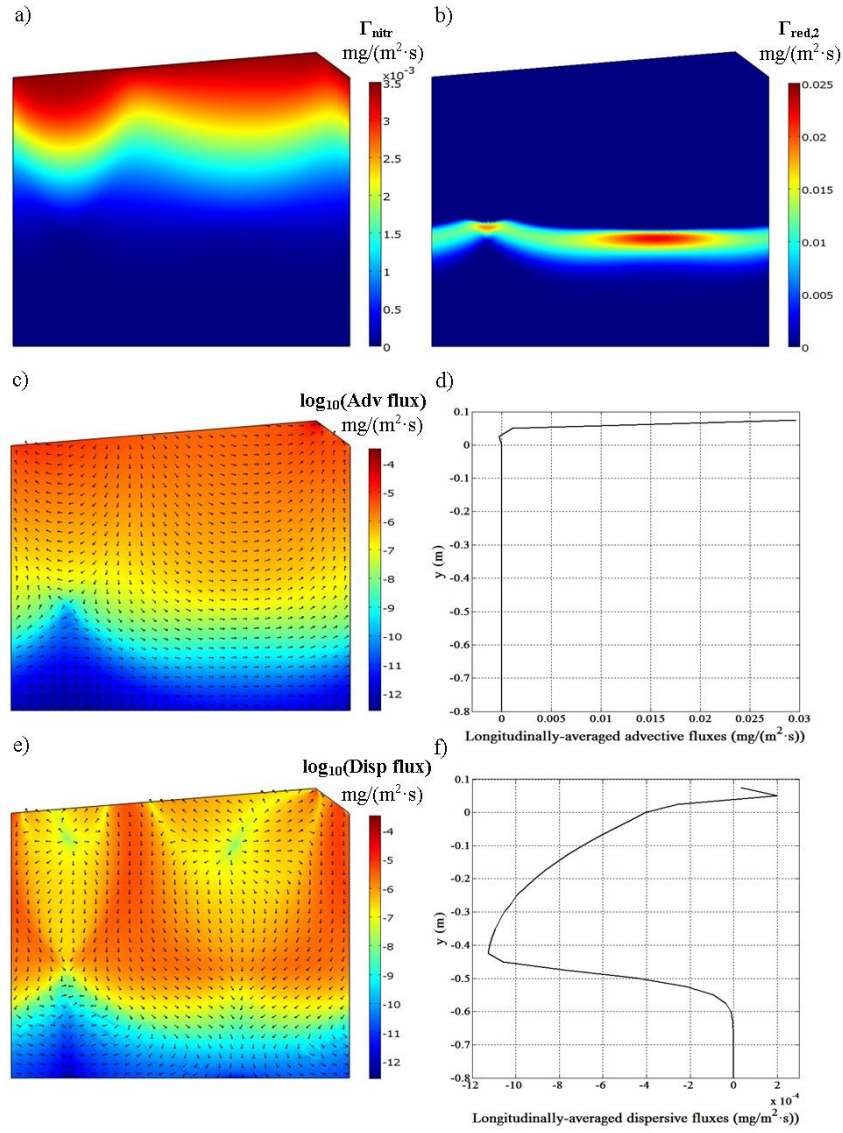
41

Figure 2.8: Nitrification and denitrification rates (Figures 2.8a, 2.8b), logarithmic values and longitudinally-averaged vertical profiles of advective (Figures 2.8c, 2.8d) and dispersive (Figures 2.8e, 2.8f) fluxes of nitrate (case 2). Vectors are only indicative of flux direction.

Table 2.3: IAR, ID and IN rates for cases 1, 2 and 3.

Case	IAR	ID	IN	ID/IN
-	μg/(m·s)	μg/(m·s)	μg/(m·s)	-
1	106	31.4	55.9	0.56
2	49.5	1.14	0.87	1.31
3	6.14	0	1.08	0

depth, for lack of ammonium. For this reason nitrate concentrations show an increase with depth up to 60 cm of depth, while they keep a constant value under that layer. As seen for case 1, the hyporheic zone behaves as a net nitrate source because of the strong nitrate dispersive transport (induced by nitrate production), upward directed, near the bed surface.

The different behavior of the hyporheic zone in the three cases is clearly underlined by the values of the Integrated oxygen Aerobic Respiration rates (IAR) and the Nitrification (IN) and Denitrification (ID) rates (see Table 2.3)

$$IAR = \int_{A_s} \Gamma_{red,1} \cdot \mathrm{d}A, \tag{2.24}$$

$$IN = \int_{A_s} \Gamma_{nitr} \cdot \mathrm{d}A, \tag{2.25}$$

$$ID = \int_{A_s} \Gamma_{red,2} \cdot \mathrm{d}A, \tag{2.26}$$

where A_s is the subsurface domain area, i.e. the volume of sediments per unit stream width.
Table 2.3 shows that aerobic respiration rate IAR increases with increasing in-stream concentrations of DOC (e.g., compare cases 2 and 3). In fact, increasing in-stream DOC concentration concurs to increase oxygen reduction rate $\Gamma_{red,1}$ (see Equations (2.11) and (2.12)), and thus IAR.

If we focus on nitrate, the ratio between ID and IN indicates the reactive behavior of the dune as a net sink (ID/IN > 1) or source (ID/IN < 1) of nitrate. This happens because there is no net solute flux trough the lateral boundaries due to the periodic boundary

conditions, and thus net nitrate production equals net exchange flux through the streambed. In Table 2.3 we observe that the hyporheic zone can act as a net source of nitrate in both polluted and pristine streams (cases 1 and 3), despite these cases representing two seemingly opposite chemical conditions. The DOC availability is a discriminating parameter for the degradation rates in pristine streams; high concentrations of labile DOC enhance both aerobic respiration and denitrification rates, leading to a faster removal of oxygen and a net consumption of nitrate in hyporheic sediments.

2.3.2   Impact of stream velocity

Increasing stream velocity values are considered for the three cases in Table 2.2, in order to estimate and compare the solute reaction rates, reflecting the behavior of the streambed. The stream velocity ranges from 0.21 m/s to 0.39 m/s, which correspond to Reynolds number Re between 106,670 and 195,630.

A variation of the stream velocity induces two opposite effects on solute reactions. From a hydrodynamical point of view, an increase in U implies higher inward water fluxes due to the higher pressure gradients on the dune surface. This leads to larger fluxes of substances from the stream to the sediments which can enhance reaction rates. Neverthless, hyporheic microbes have less time for performing biochemical reactions because of the lower residence time of the compounds in the streambed, potentially leading to lower reaction rates. The net effect on reaction rates depends on the interaction between these opposite factors, i.e, higher solute inputs and lower residence times (Arnon et al., 2007; Cardenas et al., 2008a).

Looking at the results (Table 2.4), it can be observed that all integrated solute reaction rates increase with the stream velocity, even if with different relative variations. In particular, the IN parameter shows a higher sensitivity to the stream velocity variations than the other ones, with consequences on the general streambed reactive behavior. These trends demonstrate that in the simulated conditions the increase of inward solute fluxes, with U, have a predominant role for the solute reaction rate, while the decrease of the residence times in the porous medium is less important.

As to the net nitrate production rate, we consider the ratio of

Table 2.4: IAR, ID and IN rates for cases 1, 2 and 3, with different stream velocities.

Case	U	IAR	ID	IN	ID/IN
-	m/s	μg/(m·s)	μg/(m·s)	μg/(m·s)	-
1	0.21	78.1	26.6	38.1	0.7
1	0.24	85.8	28.1	42.8	0.66
1	0.27	93.2	29.4	47.5	0.62
1	0.30	100	30.5	52.0	0.59
1	0.33	106	31.4	55.9	0.56
1	0.36	111	32.2	59.4	0.54
1	0.39	116	32.9	62.8	0.52
2	0.21	38.3	1.05	0.62	1.68
2	0.24	41.4	1.08	0.69	1.57
2	0.27	44.4	1.11	0.76	1.47
2	0.30	47.2	1.13	0.82	1.39
2	0.33	49.5	1.14	0.87	1.31
2	0.36	51.5	1.15	0.92	1.25
2	0.39	53.4	1.15	0.96	1.19
3	0.21	4.99	0	0.80	0
3	0.24	5.32	0	0.88	0
3	0.27	5.63	0	0.95	0
3	0.30	5.91	0	1.02	0
3	0.33	6.14	0	1.08	0
3	0.36	6.33	0	1.13	0
3	0.39	6.50	0	1.18	0

ID to IN. Figure 2.9 shows that the increase of the stream velocity does not change dramatically the streambed behavior but it clearly leads to limiting the sink role (case 2), and to enhance the source role (case 1) of the hyporheic zone. This behavior is the result of a higher sensitivity of nitrification to stream velocity, compared to denitrification.
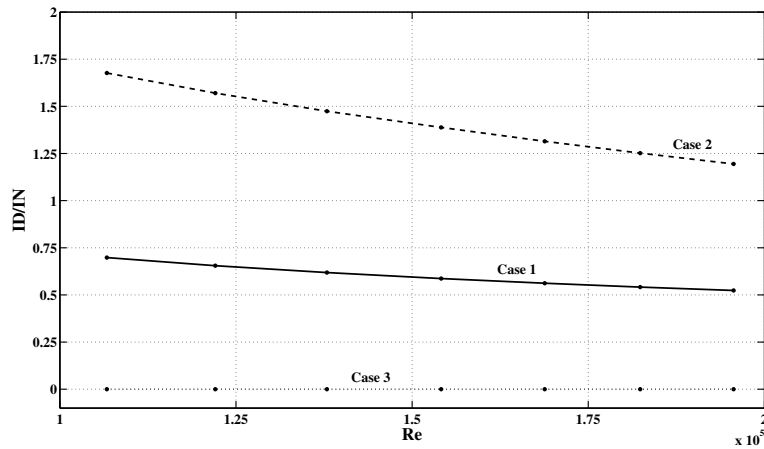
Figure 2.9: Ratio of ID to IN rates vs. Reynolds numbers for case 1 (solid line), case 2 (dashed line) and case 3 (dotted line).

2.3.3 Impact of sediment hydraulic and transport properties

We focus on the pristine stream configuration with no DOC limitation (case 2). Although recently it has been demonstrated that sediment permeability heterogeneity influences hyporheic exchange (Sawyer and Cardenas, 2009), in this section the role of permeability is investigated, under the hypothesis of homogeneity, for the sake of simplicity. The stream velocity U is set to the constant value of 0.27 m/s, while the sediment permeabilities and dispersivities are varied to investigate the influence of the size of sediment grains (see Table 2.5). Since dispersivity is proportional to the sediment grain size, d_g, and permeability scales with d_g^2, it follows that a ten-fold increase in κ results in approximately a three-fold increase in α_L. Again, values of the transversal dispersivities α_T are

46

Table 2.5: IAR, ID and IN rates for case 2, with different permeabilities and dispersivities.

$10^{11} \cdot \kappa$ m^2	α_L mm	α_T mm	IAR $\mu g/(m{\cdot}s)$	ID $\mu g/(m{\cdot}s)$	IN $\mu g/(m{\cdot}s)$	ID/IN -
1.00	1.00	0.10	13.2	0.54	0.18	3.09
5.00	2.20	0.22	33.1	0.97	0.52	1.88
10.0	3.00	0.30	44.4	1.11	0.76	1.47
50.0	6.60	0.66	76.9	1.49	1.58	0.94

chosen as a tenth of the longitudinal ones. The results underline a marked effect of the permeability on the solute spatial distribution (see Figure 2.10), with less steep fronts corresponding to higher values of permeability and dispersivity. The increase of κ, α_L and α_T results in more efficient advective and dispersive transport and enhanced solute penetration. For $\kappa = 10^{-11}$ m^2 DOC degradation is fast and the compound is completely removed within the first 30 cm of depth (Figure 2.10a), while for $\kappa = 5 \cdot 10^{-10}$ m^2 high DOC values (38 mg/L) are still present at the bottom of the streambed (Figure 2.10d). It is also interesting to observe the different streambed aerobic conditions in the opposite cases, with the aerobic zone confined in the shallower layers for the low permeability case and filling almost all the porous medium for the high permeability case. The integrated reaction rates show an increase with increasing sediment permeability (Table 2.5), with different sensitivities. This behavior is caused by the higher nutrient supply from the stream with increasing permeability, and is similar to the effect of increasing stream velocity. Values of IN show that nitrification, more than denitrification, is sensitive to permeability, which leads to a shift from the hyporheic zone acting as a net nitrate sink (ID/IN > 1) to source (ID/IN < 1) with increasing κ.

2.4   Discussion

The solute spatial distribution in the hyporheic zone is due to a strong interplay of both hydraulic and biogeochemical processes.
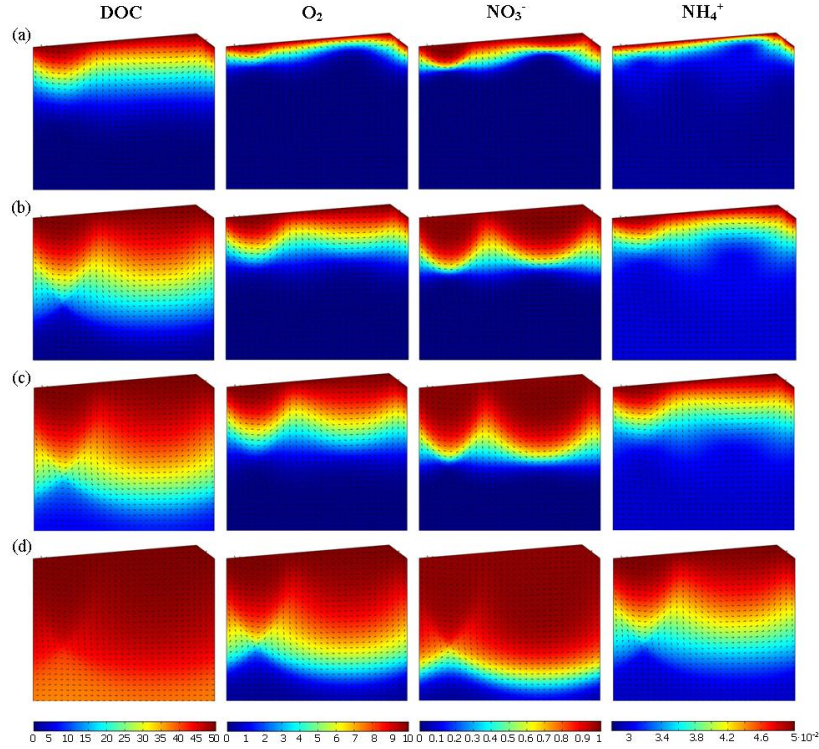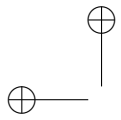
Figure 2.10: Solute spatial distributions for case 2 (see Table 2.2), with stream velocity $U = 0.27$ m/s and sediment permeabilities $\kappa = 10^{-11}$m^2 (Figure 2.9a), $5 \cdot 10^{-11}$m^2 (Figure 2.9b), 10^{-10}m^2 (Figure 2.9c), $5 \cdot 10-10$m^2 (Figure 2.9d). DOC reaction rate is $k_{DOC} = 5 \cdot 10^{-6}$s^{-1}, nitrification rate is $kn = 5 \cdot 10-6$ L/(mg $\cdot$ s). All concentrations are expressed in mg/L.

Nutrients enter the sediments because of pressure-induced water exchanges, and there they are both transported by advective and dispersive fluxes, and then biochemically transformed by hyporheic microbiota. So, a variation of the transport conditions or the chemical kinetics, induced by different stream and sediment characteristics, can have a direct influence on the reaction potential of the streambed, with ecological implications. If we focus on the hyporheic fauna, the exchanges of water, nutrients and organic matter through the streambed and the chemical concentrations in the sediments are fundamental for microbiota and invertebrates.

48

Our simulations have shown that the stream water quality can strongly affect the biogeochemical reactions. In general, the streambed always acts as a sink of DOC, oxygen and ammonium, while nitrate, that is subject to production and consumption reactions, displays a more complex behavior. In the considered cases, high in-stream concentrations of solutes have been shown to enhance nitrification process leading to strong nitrate production in the porous medium. In these conditions the hyporheic zone behaves as a nitrate source for the stream. In pristine streams nitrate fate has proved to be strictly linked to DOC availability. A scarcity of DOC can limit denitrification and prevent nitrate removal, leading to a streambed acting as a nitrate source. Instead, high concentrations of DOC favour denitrification and lead to a net nitrate consumption.

Stream velocity and sediment permeability have displayed a direct effect on transport phenomena. Increasing stream velocity implies larger solute fluxes to sediments but also lower residence times of the compounds in the hyporheic zone and a lower time for reactions. In our simulations, the higher solute supply clearly prevails over the lower residence times, since all reaction rates increase with stream velocity. In particular, nitrification appears to be more sensitive to changes in stream velocity than denitrification. The consequence is that high stream velocities damp the sink role and enhance the source role of the streambed. The hydraulic properties of sediments have a similar influence on solute spatial distribution. Higher values of permeability improve the transport efficiency and increase reaction rates, strongly affecting the reactive behavior of the hyporheic zone. In particular, high-permeability sediments enhance nitrate production and can induce a switch from nitrate sink to source behavior.
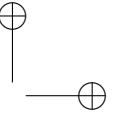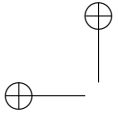
Chapter 3

Impact of small-scale permeability heterogeneity on chemical zonation in the hyporheic zone

3.1 Introduction

Aquatic sediment hosts coupled porewater flow and biogeochemical reactions that mediate water quality across the fluvial corridor including adjacent alluvial aquifers. However, the effect of small-scale variations in sediment hydraulic properties on nutrient transformation occurring within the sediment is poorly understood.

Some researchers have investigated the interactions between hydrodynamical and biogeochemical processes in the hyporheic zone (e.g., Boano et al., 2010; Bardini et al., 2012; Gomez et al., 2012; Kessler et al., 2012; Zarnetske et al., 2012), assuming homogeneous permeability conditions for the sediments. Only a small number of works have studied the role played by sediment heterogeneity on hyporheic exchange (Cardenas et al., 2004; Marion et al., 2008a; Salehin et al., 2004; Sawyer and Cardenas, 2009) but they did not take into account the biogeochemical reactions. Therefore, understanding the impact of sediment heterogeneity on both advective
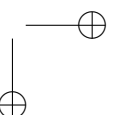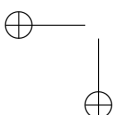
and dispersive fluxes and hyporheic chemical reactions has been elusive.

The aim of this chapter is to investigate the effect of sediment heterogeneity on reactive solute spatial distribution in a rippled riverbed, by taking into account both hydraulic and biochemical processes. The cross-bedded sediments examined here are typical of lowland rivers, with no armoring layers. To isolate the effects of heterogeneous permeability fields on reactive transport, we will not consider heterogeneity in solid sediment chemistry such as organic matter content. We will consider two different bedform configurations and compare the numerically simulated chemical distributions resulting from the heterogeneous permeability fields with two equivalent anisotropic homogeneous cases. We will focus on the same compounds of the previous chapter, i.e., DOC, oxygen, nitrate and ammonium, which are among the most important substances for stream ecology.

3.2   Permeability data sets

We consider two permeability (κ) fields, from the Brazos River and the Massillon Sandstone (USA). The first data set was created by Sawyer and Cardenas (2009) from an image of climbing ripple deposits of the Brazos River near Wallis, in Texas, by assuming a relationship between the gray colour scale and the permeability values. These sediments are ripple-laminated and bimodal in composition (see Figure 3.1a). The angle of ripple climb varies from 15° at the bottom domain to 40° near the top domain, while the $\ln(\kappa)$ values range between -27.5 and -22.9, typical of sand and organic-rich silt, with a variance of 1.

The Massillon conductivity field results from high-resolution direct permeability measurements conducted by Tidwell and Wilson (2000) on a two-dimensional face of a block from the Massillon Sandstone, in Ohio. The structure is composed of cross-stratified sets bounded by subhorizontal, undulatory to planar surfaces and it is moderately well sorted (Figure 3.1b). To correct for permeability reduction due to diagenetic alterations, we uniformly scale the permeability values by a factor of 10 (Sawyer and Cardenas, 2009). The final $\ln(\kappa)$ varies between -26.4 and -23.7 values, characteristic

a)

b)
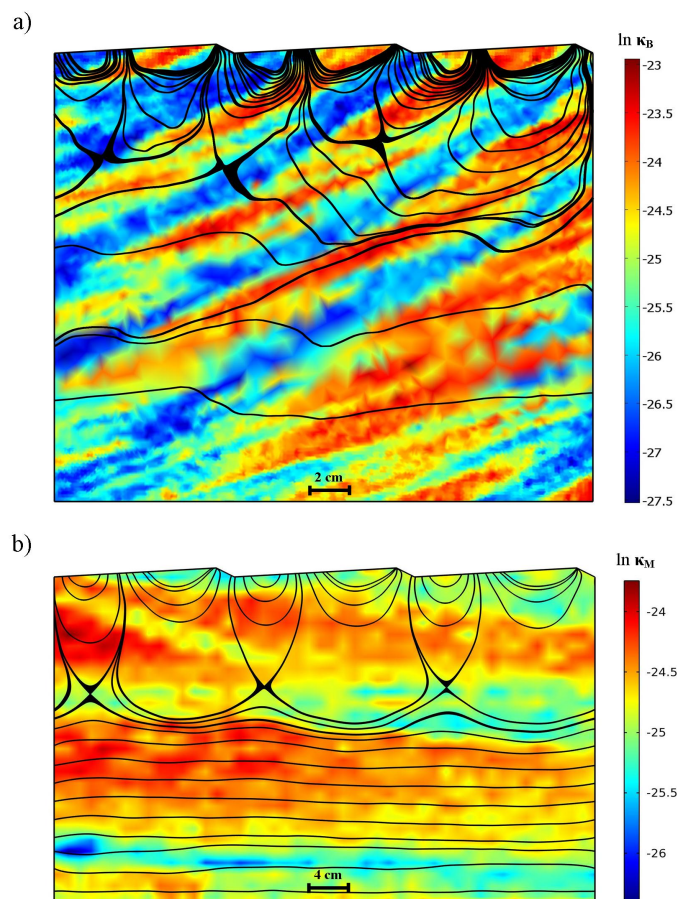
Figure 3.1: Brazos River and Massillon Sandstone permeability fields. Streamlines are shown in black. Flow in surface water (not shown) is from left to right.

of sands, with a variance of 0.15.

The two datasets are representative, respectively, of moderate and mild variation in permeability. The $\ln(\boldsymbol{\kappa})$ variances are small compared to others measured or simulated in previous studies of heterogeneous fluvial sediments at larger spatial scales (e.g., Genereux et al., 2008; Kalbus et al., 2009). Instead, we consider a permeability structure at the smaller scale of fluvial bedforms and corresponding to a single depositional facies.

From the heterogeneous permeability fields we obtain the equivalent homogeneous anisotropic permeability tensors $\boldsymbol{\kappa_B}$ (for Brazos) and $\boldsymbol{\kappa_M}$ (for Massillon) by applying the method of Durlofsky (1991)

$$\boldsymbol{\kappa_B} = 10^{-11} \times \begin{bmatrix} 1.39 & 0.259 \\ 0.259 & 1.07 \end{bmatrix} \mathrm{m}^2 \tag{3.1}$$

$$\boldsymbol{\kappa_M} = 10^{-11} \times \begin{bmatrix} 2.07 & -0.00376 \\ -0.00376 & 1.90 \end{bmatrix} \mathrm{m}^2 \tag{3.2}$$

These permeability tensors will be used to compare solute dynamics in the hyporheic zone in equivalent homogeneous conditions.

3.3   Biogeochemical and hydraulic model

The sediment-water interface is shaped in order to represent a rippled riverbed, with three two-dimensional repeating bed forms, triangular in shape. Bed form size differs for Massillon and Brazos cases (Table 3.1), while the length to height ratio is kept constant. A Cartesian reference system is adopted, with x and y as the streamwise and upward coordinates, respectively, and the axis origin is placed at the first ripple trough.

Table 3.1: Geometrical and hydraulic model parameters

	Massillon case	Brazos case
Bed form length L (m)	0.2	0.1
Bed form height H (m)	0.01	0.005
Mean stream velocity U (m/s)	0.1	0.1
Stream depth d (m)	0.2	0.2
Porosity θ (-)	0.3	0.25
Longitudinal dispersivity α_L (mm)	1	1
Transverse dispersivity α_T (mm)	0.1	0.1
Molecular diffusion coefficient D_{mol} (m^2/s)	5×10^{-11}	5×10^{-11}

We focus on the chemical compounds studied in Chapter 2, i.e.,

DOC, oxygen, nitrate and ammonium and we recall the biogeo-chemical reactions presented in Table 2.1, i.e., aerobic respiration, denitrification and nitrification.

The steady-state advective flow in the sediments **q** is simulated by solving the groundwater flow equations

$$\mathbf{q} = -\frac{\gamma\boldsymbol{\kappa}}{\mu}\nabla h \qquad \nabla \cdot \mathbf{q} = 0, \qquad (3.3)$$

where γ is the specific weight of water, μ is the dynamic viscosity of water, $\boldsymbol{\kappa}$ is the permeability tensor, h is the hydraulic head and $\mathbf{q} = (q_x, q_y)$ is the Darcian velocity vector.

The hyporheic advective flow field **q** (Equation (3.3)) is then coupled with the overall reaction rates R_s (Equations (2.16)–(2.19)) and the hydrodynamic dispersion tensor **D** (Equation (2.21)) in order to define the solute reactive transport equations in steady-state conditions (Equations (2.20)). A detailed explanation of the model Equations (2.16) - (2.9) is present in Chapter 2.

Lateral boundaries are periodic in both head and concentration, with a prescribed head drop representing the river slope. The lower boundary is assigned a no-flow condition for fluid and solute. On the upper boundary we prescribe a constant concentration value (i.e., the in-stream concentration) at inlet zones and a negligible dispersive flux at outlet zones. Head along the top boundary is estimated by Sawyer and Cardenas (2009) through open channel flow simulations, by numerically solving, in steady-state conditions, the Reynolds-Averaged Navier-Stokes (RANS) equations for incompressible and homogeneous fluids, with the $k - \omega$ closure scheme (for further details see Cardenas and Wilson, 2007b).

The governing equations of the biogeochemical model are numerically solved in Comsol, a generic multiphysics finite element solver, with adaptive meshing and error control. For both Brazos and Massillon cases we consider two opposite chemical conditions: a polluted one, with higher in-stream solute concentrations ($C_{DOC} = 60$ mg-C/L, $C_{O_2} = 10$ mg/L, $C_{NO_3^-} = 8$ mg/L, $C_{NH_4^+} = 5$ mg/L), and a pristine one, with lower in-stream solute concentrations ($C_{DOC} = 2$ mg-C/L, $C_{O_2} = 10$ mg/L, $C_{NO_3^-} = 1$ mg/L, $C_{NH_4^+} = 0.05$ mg/L). The physical and hydraulic parameters used in the simulations are listed in Table 3.1. Since the aim of the work is to investigate the effect of permeability heterogeneity on

hyporheic flow and reactions, we compare the results of simulations with heterogeneous and equivalent homogeneous permeabilities for both Brazos and Massillon cases.

3.4   Results

Sediment heterogeneity affects the advective flow field in both Brazos and Massillon cases (Figures 3.2-3.5). In general, permeability heterogeneity produces more irregular flow cells within shallow sediments, promotes deeper exchange, and longer path lengths. Details on the flow behavior and implications for conservative solute transport are available in Sawyer and Cardenas (2009).

Inspection of the streambed chemical zonation shows marginal effects of sediment heterogeneity in both the Brazos and Massillon sediments, as shown in Figures 3.2 and 3.3 for the polluted stream case. Results for the pristine case (see Figures 3.4 and 3.5) are analogous. Concentration fronts are quite similar in size and shape for heterogeneous and homogeneous permeability conditions. The main reason is that, despite the relevant variations in fluid flow paths, the residence time distributions are fairly similar for these cross-bedded heterogeneous sediments and their equivalent homogeneous media (Sawyer and Cardenas, 2009). This finding is also confirmed by the net solute removal/production rates in the streambed (see Tables 3.2 and 3.3).
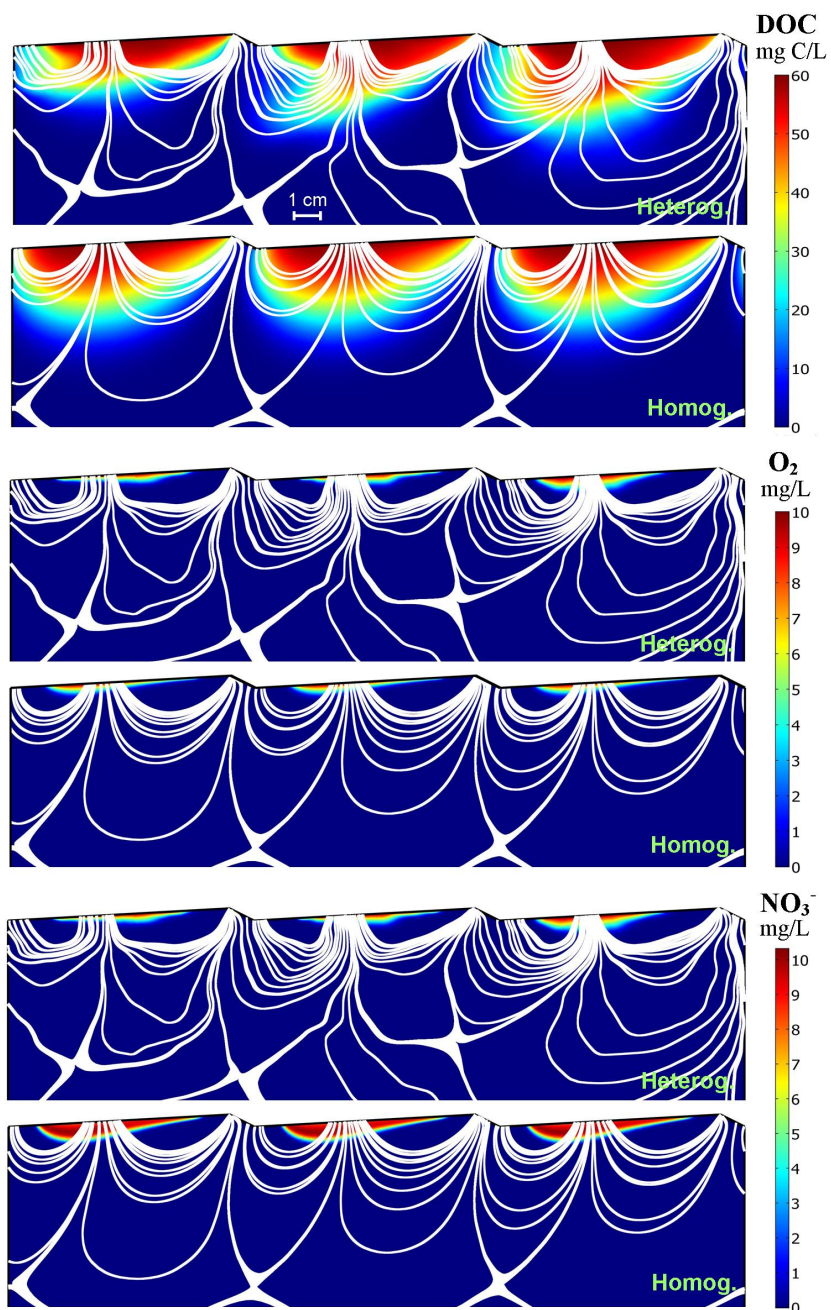
Figure 3.2: Steady-state solute spatial distribution for Brazos River sediments in heterogeneous and homogeneous conditions (polluted stream case). Streamlines are shown in white.
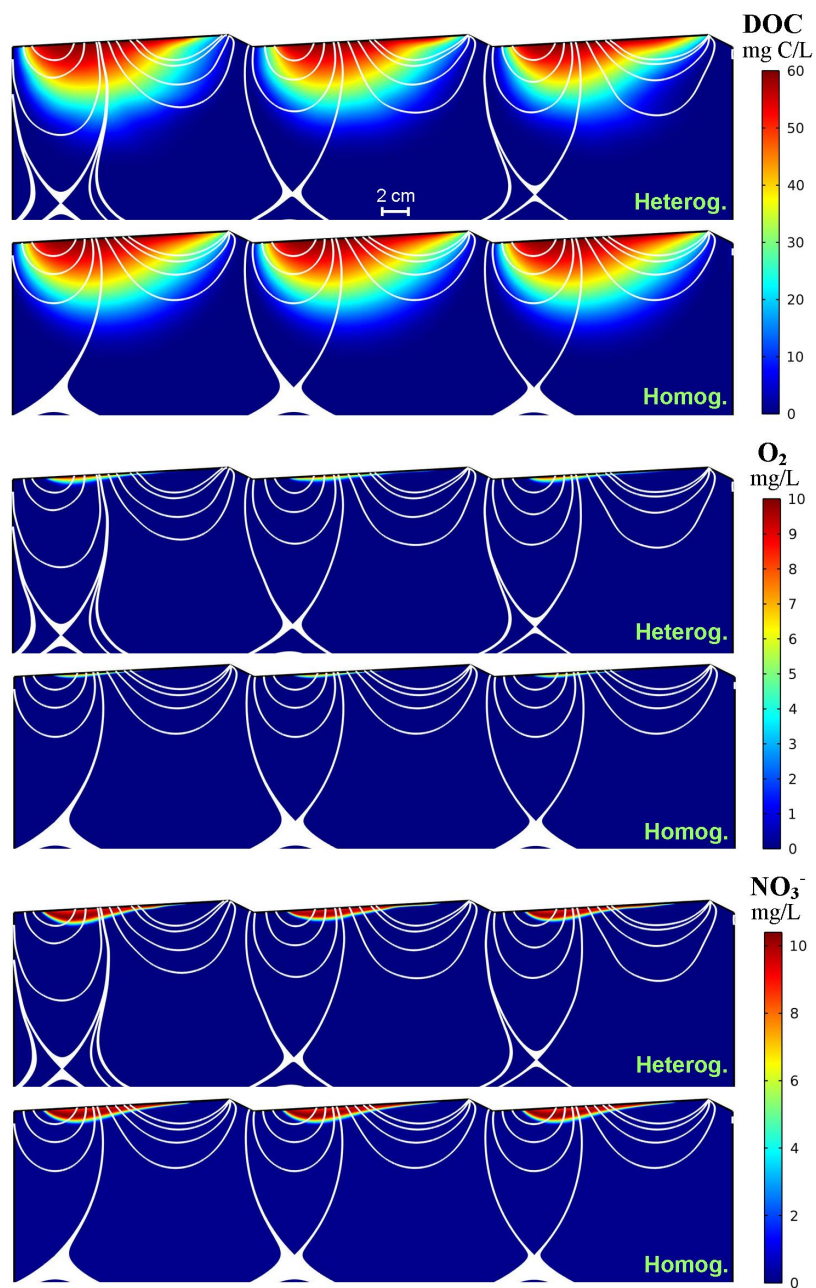
Figure 3.3: Steady-state solute spatial distribution for Massillon Sandstone sediments in heterogeneous and homogeneous conditions (polluted stream case). Streamlines are shown in white.
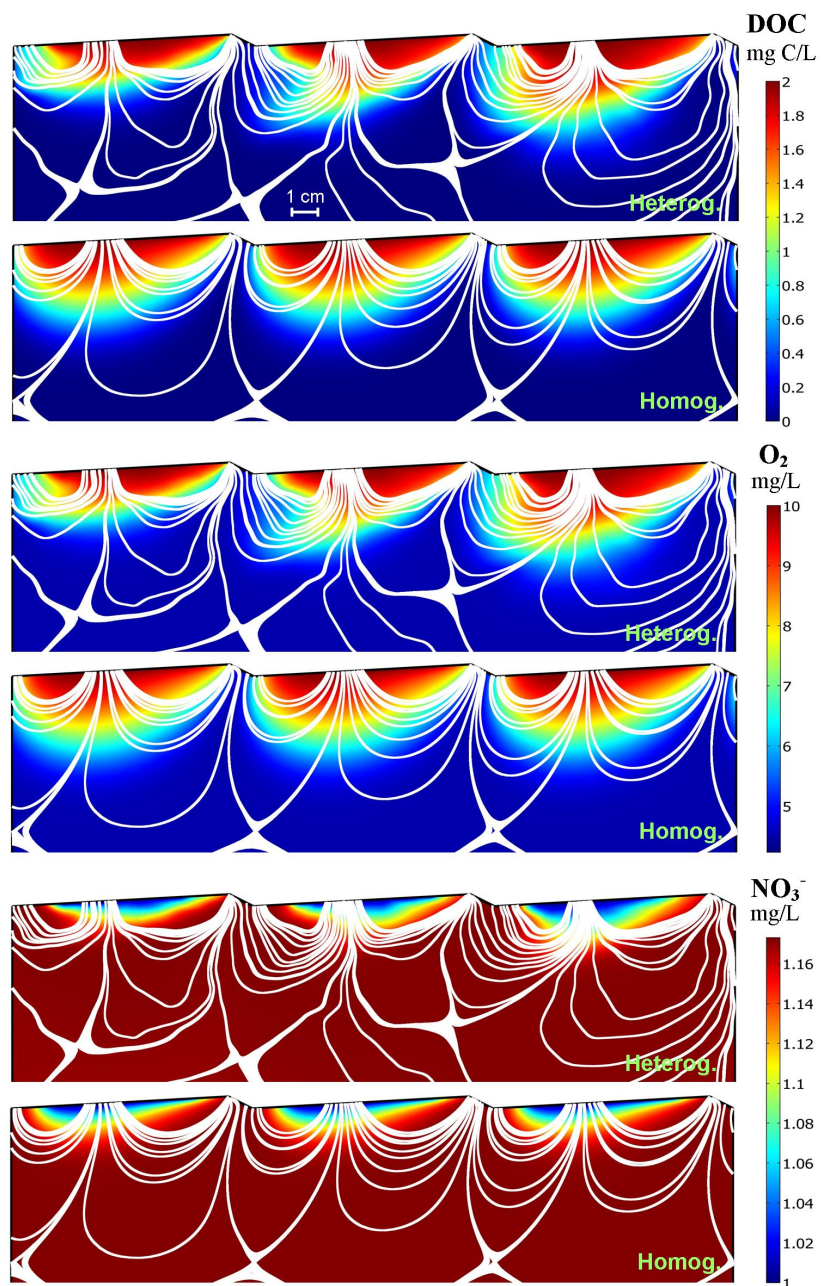
Figure 3.4: Steady-state solute spatial distribution for Brazos River sediments in heterogeneous and homogeneous conditions (pristine stream case). Streamlines are shown in white.

59
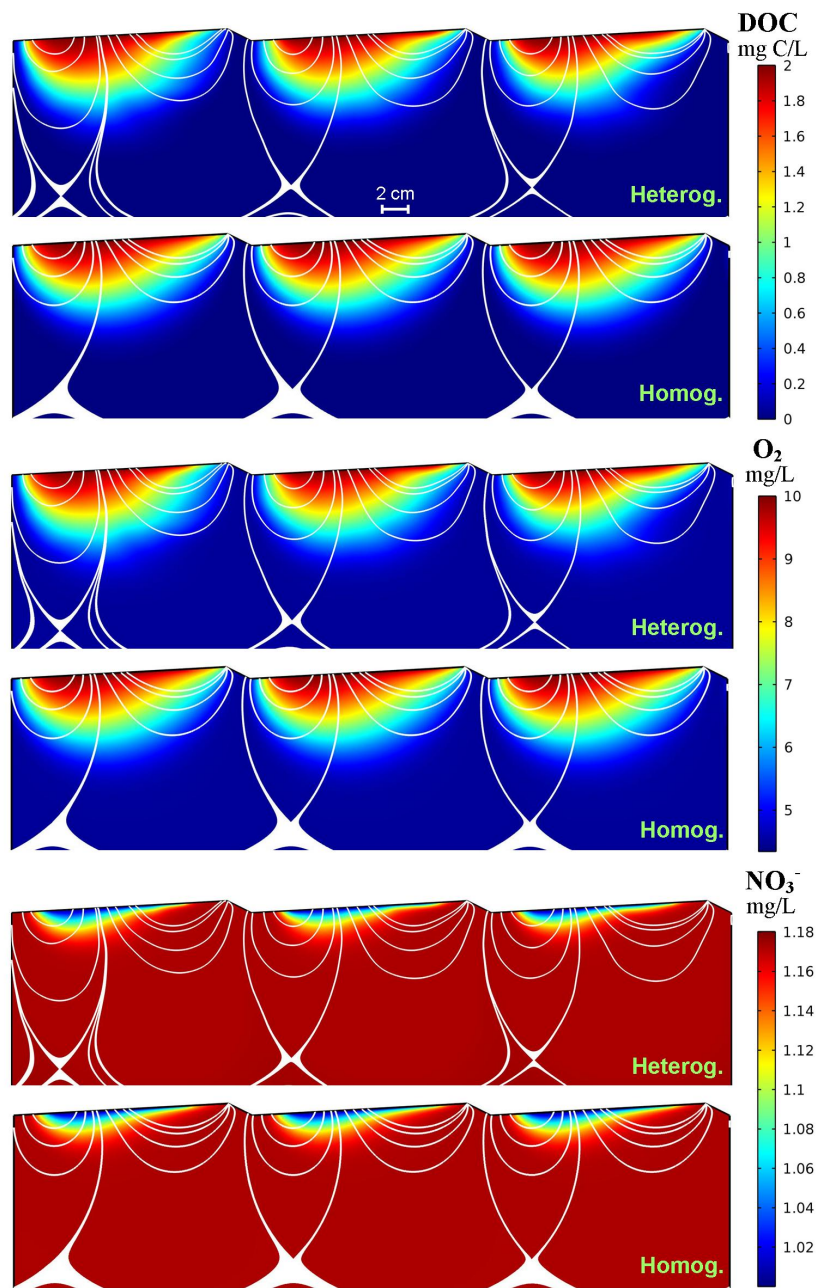
Figure 3.5: Steady-state solute spatial distribution for Massillon Sandstone sediments in heterogeneous and homogeneous conditions (pristine stream case). Streamlines are shown in white.

Table 3.2: Solute reaction rates for heterogeneous and homogeneous Brazos River sediments in the pristine and polluted river cases. Positive and negative values are indicative of net solute production and removal, respectively. The relative variations of net rates in heterogeneous conditions compared to the equivalent homogeneous conditions are also reported.

	Heterogeneous case rates mg/(m·s)	Homogeneous case rates mg/(m·s)	Rate difference %
Pristine river			
DOC	-1.46×10^{-5}	-1.63×10^{-5}	-10.5
O_2	-4.22×10^{-5}	-4.67×10^{-5}	-9.6
NO_3^-	$+3.12 \times 10^{-6}$	$+3.05 \times 10^{-6}$	2.4
NH_4^+	-9.06×10^{-7}	-8.85×10^{-7}	2.4
Polluted river			
DOC	-4.38×10^{-4}	-4.90×10^{-4}	-10.5
O_2	-2.67×10^{-4}	-2.47×10^{-4}	8.1
NO_3^-	-1.14×10^{-4}	-1.05×10^{-4}	8.7
NH_4^+	-2.28×10^{-5}	-2.08×10^{-5}	9.8

61

Table 3.3: Solute reaction rates for heterogeneous and homogeneous Massillon Sandstone sediments in the pristine and polluted river cases. Positive and negative values are indicative of net solute production and removal, respectively. The relative variations of net rates in heterogeneous conditions compared to the equivalent homogeneous conditions are also reported.

	Heterogeneous case rates mg/(m·s)	Homogeneous case rates mg/(m·s)	Rate difference %
Pristine river			
DOC	-4.61×10^{-5}	-5.16×10^{-5}	-10.6
O_2	-1.30×10^{-4}	-1.46×10^{-4}	-11.0
NO_3^-	$+6.84 \times 10^{-6}$	$+8.15 \times 10^{-6}$	-16.1
NH_4^+	-1.99×10^{-6}	-2.37×10^{-6}	-16.1
Polluted river			
DOC	-1.38×10^{-3}	-1.55×10^{-3}	-10.6
O_2	-5.27×10^{-4}	-6.17×10^{-4}	-14.6
NO_3^-	-2.41×10^{-4}	-3.00×10^{-4}	-19.7
NH_4^+	-4.44×10^{-5}	-5.24×10^{-5}	-15.2

The reaction rate differences between homogeneous and heterogeneous conditions are higher in the Massillon sediments (almost 20% for nitrate), with the exception of DOC, which varies the same amount (10%) in all cases. In general, these results indicate that bedform-scale heterogeneity typical of lowland rivers does not dramatically alter nutrient reactions in both the Brazos and the Massillon cases.

The role of the streambed in nutrient transformation appears to be fairly influenced by water fluxes across the sediment-water interface. The heterogeneous Massillon case has slightly lower water fluxes across the sediment-water interface than equivalent homogeneous case (Sawyer and Cardenas, 2009), and all reaction rates are correspondingly slower (Table 3.2). The influence is less evident for Brazos sediments, where the slight increase of hyporheic flux in heterogeneous conditions (Sawyer and Cardenas, 2009) corresponds on the one hand to an increase of nitrate and ammonium reaction rates and on the other hand to a decrease of DOC and oxygen rates (Table 3.3). This behavior indicates an influence, albeit small, of the structure of the flow field.

Another important consideration is the effect of river water quality on the role of the streambed in nitrogen cycling. For example, the pristine river configurations lead to a net nitrate production, as confirmed by the positive values of the nitrate reaction rates in the sediments for both the heterogeneous and homogeneous conditions (Tables 3.2 and 3.3). In fact, the low DOC concentrations limit the aerobic respiration rate and maintain higher oxygen concentrations than the limiting value for denitrification. Thus, nitrate is not removed by denitrification and is produced by nitrification, and its concentrations increase with depth (see Figures 3.4 and 3.5). Therefore, in this case where nutrients are relatively scarce, the sediments represent a nitrate source.
In contrast, the polluted river configurations lead to a net nitrate removal, as shown by the negative nitrate reaction rates. Nitrate concentration increases with depth in the shallower layers of the sediments, where nitrification prevails, and it decreases below a specific depth, where denitrification prevails, until being completely consumed (Figures 3.2 and 3.3). The interaction between nitrification and denitrification rates in the whole domain eventually results in a nitrate sink behavior of the riverbed. This last result differs

from the one presented by Bardini et al. (2012), who found a nitrate source behavior for the same in-stream concentrations as in the polluted river configuration but with bedforms of larger size. The explanation of this difference is that the larger bedforms enhanced water exchange through the streambed, with higher oxygen influxes to the sediments, preventing denitrification. This comparison further confirms that nutrient fate in streambeds is controlled by non-trivial and non-linear interactions among water chemistry, transport processes, and microbial reactions.

3.5 Discussion

Though flow fields in both Brazos and Massillon sediments are altered by moderate permeability heterogeneity, solute reaction rates and concentrations in riverbed sediment are similar. Thus, sediment hetereogeneity at the bedform scale does not strongly influence streambed nutrient dynamics.

These results are coherent with those of Sawyer and Cardenas (2009), who found that permeability heterogeneity induced moderate differences in the distributions of residence times despite relevant variations in water flow paths. Thus, residence times are a better indicator and predictor of subsurface reactions than porewater flow patterns, at least in the case of homogeneous solid sediment biochemistry. This supports the proposed approach by Zarnetske et al. (2011) and Gomez et al. (2012) of using primarily the ratio of characteristic residence and reaction times to predict the biogeochemical role and regime of aquatic sediment.

The pristine river case, with low in-stream nitrate and DOC concentrations, has proved to induce a net nitrate production in the sediments, while the polluted one has led to a net nitrate removal. The same nitrate sink/source behavior has been found for heterogeneous and homogeneous conditions, suggesting that variations of permeability at the bedform scale do not measurably alter the role of streambeds in nutrient cycling. This is fortunate because adequate representation of nitrogen cycling in shallow streambed sediment is possible without detailed information about the small-scale permeability structure.
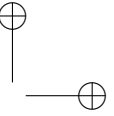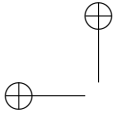
Conclusions

This thesis has been concerned with the water and solute exchanges across the riverbed and the chemical reactions active in the hyporheic zone. Specifically, we have focused on the strong interplay between hydraulic and biogeochemical processes and their effects on water-borne solute dynamics in the hyporheic sediments. We have developed a numerical model for simulating solute transport and reaction in streambeds, characterized by the presence of bedforms (dunes and ripples) and by different hydraulic and physico-chemical peculiarities. The chemical compounds of interest were DOC, oxygen, nitrate and ammonium.

As expected, all simulations have demonstrated a net removal of DOC, oxygen and ammonium in the streambed. Instead, the picture has proved to be further complicated for nitrate, since it takes part in two antagonistic reactions, i.e., nitrification (as a product) and denitrification (as a reactant). Thus, the hyporheic zone can act as a nitrate source or sink depending on stream and sediment properties.

Stream water quality has shown to highly influence the nitrate streambed behavior in our simulations, by directly affecting both solute fluxes to the streambed and reaction rates. We have estimated a net nitrate production in the streambed in polluted streams, while we have underlined two opposite behaviors, depending on DOC in-stream concentration, in pristine streams. In particular, a scarse or large availability of DOC has proved to limit or enhance denitrification and favor a net nitrate production or removal, respectively. Instead, variations of stream velocity and sediment permeability have demonstrated to slightly affect the streambed nitrate behavior. Both parameters influence transport phenomena by acting on both solute fluxes and residence times in
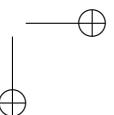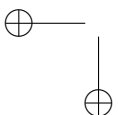
the hyporheic zone. An increase of stream velocity implies, on the one hand, larger downwelling solute fluxes but, on the other hand, lower times available for hyporheic reactions. The predominance of one effect on the other determines the increase or decrease of reaction rates. In the considered cases, solute fluxes have proved to prevail on residence times since all solute reaction rates have displayed an increase with stream velocity, even if with different sensitivities. In particular, nitrification has demonstrated to be more sensitive than denitrification. Thus, in our simulations, the stream velocity has damped the nitrate removal and enhanced nitrate production in the streambed. In a similar way, a high permeability of the sediments has favored the nitrate source behavior of the hyporheic zone.

In the second part of the work we have investigated the effect of permeability heterogeneity on solute transport in rippled streambeds. We have focused, specifically, on configurations typical of lowland rivers, with no armoring layers and no significant stratification. Specifically, the chemical spatial distributions resulting from two heterogeneous permeability fields have been compared with two equivalent anisotropic cases. Results have shown that, despite stark differences in the flow fields, little variations have occured in the reactive transport patterns and in the bulk reaction rates of all substances. Besides, focusing on nitrate, the sink/source function of the streambed has been similar in heterogeneous and homogeneous conditions. Thus, sediment heterogeneity at the bedform scale have demonstrated to not strongly affect nutrient dynamics in the hyporheic sediments. The reason is that reactions are ultimately controlled by characteristic or bulk residence times which are similar for the heterogeneous and homogeneous cases. These results make possible to apply predictive models based solely on relative ratios of residence times and reactive time scales for the representation of nitrogen cycling in shallow streambeds of lowland rivers, at least for variations of streambed permeability of moderate intensity.

Appendix A

Notation

The symbols and notation used in this thesis are listed below.

Acronyms

CFD	Computational Fluid Dynamics;
CTRW	Continuous Random Walk Approach;
DOC	Dissolved Organic Carbon;
IAR	Integrated oxygen Aerobic Respiration rate;
ID	Integrated Denitrification rate;
IN	Integrated Nitrification rate;
RANS	Reynolds-Averaged Navier Stokes;
RTD	Residence Time Distribution;
STIR	Solute Transport In Rivers;
TOC	Total Organic Carbon;
TSM	Transient Storage Model.

Roman letters

Lower case

d Stream mean water depth (m);

d_g Sediment grain size (m);

f_i Fraction of electrons consumed by the i-th reduction

           half-reaction (-);

g Earth gravitational acceleration (m/s^2);

h Hydraulic head (m/s^2);

i_b Streambed slope (-);

k Turbulent kinetic energy (m^2/s^2);

k_{DOC} DOC decay constant (s^{-1});

k_n Second-order nitrification rate, (L/(mol·s));

d Stream mean water depth (m);

$\mathbf{q}$ Darcian velocity vector (m/s);

q_i, q_j Darcian velocity vector components (m/s);

r_1 Aerobic respiration index (-);

r_2 Denitrification index (-);

r_3 Nitrification index (-);

$u_i^{'}$, $u_j^{'}$ Turbulent velocity components in x_i and x_j directions (m/s);
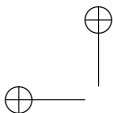
$-\overline{u'_j u'_i}$ Mean strain rate (m²/s²);

x Streamwise coordinate (m);

x_{max} Horizontal coordinate of the terminal point of the dune (m);

x_{min} Horizontal coordinate of the initial point of the dune (m);

y Upward coordinate (m);

t Time (s).

Upper case

A_s Subsurface domain area (m²);

C_{DOC} DOC concentration (mol/L);

$C_{DOC,0}$ DOC in-stream concentration (mol/L);

C_i Concentration of the i-th reaction electron acceptor (mol/L);

$C_{i,lim}$ Limiting concentration of the i-th reaction electron acceptor (mol/L);

C_{O_2} Oxygen concentration (mol/L);

$C_{O_2,0}$ Oxygen limiting concentration (mol/L);

$C_{O_2,lim}$ Oxygen limiting concentration (mol/L);

$C_{NH_4^+}$ Ammonium concentration (mol/L);

$C_{NH_4^+,0}$ Ammonium in-stream concentration (mol/L);

$C_{NO_3^-}$ Nitrate concentration (mol/L);

$C_{NH_3^-,0}$ Nitrate in-stream concentration (mol/L);

$C_{NO_3^-,lim}$ Nitrate limiting concentration (mol/L);

C_s Concentration of the chemical s (mol/L);

D   Hydrodynamic dispersion tensor (m^2/s);

$D_{i,j}$ Hydrodynamic dispersion tensor component (m^2/s);

D_{mol} Molecular diffusion coefficient (m^2/s);

H Bedform height (m);

L Bedform length (m);

L_c Bedform crest position (m);

P Water pressure in stream and sediments (Pa);

R_{DOC} DOC reaction rate (mol/(L·s));

R_{O_2} Oxygen reaction rate (mol/(L·s));

$R_{NH_4^+}$ Ammonium reaction rate (mol/(L·s));

$R_{NO_3^-}$ Nitrate reaction rate (mol/(L·s));

Re Reynolds number (-);

S_{ij} Strain rate tensor (s^{-1});

U Mean stream velocity (m/s);

U_i, U_j Time-averaged stream velocity components in x_i (i.e., x)

             and x_j (i.e., y) directions (m/s).

Greek letters

Lower case

α Closure coefficient (-);

α_i Parameter of i-th reduction limitation (-);

α_L Longitudinal dispersivity (m);

α_T Transversal dispersivity (m);

β Closure coefficient (-);

β^* Closure coefficient (-);

β_i ratio between the moles of transferred electrons per mole of oxidized DOC and the moles of electrons per mole of reduced compound in the i-th reaction (mol/mol);

γ Specific weight of water (N/m^3);

δ_{ij} Kronecker delta;

ϵ Turbulence dissipation rate (m^2/s^3);

κ Isotropic homogeneous sediment permeability (m^2);

κ Sediment permeability tensor (m^2);

$\kappa_{\mathbf{B}}$ Brazos sediment permeability tensor (m^2);

$\kappa_{\mathbf{M}}$ Massillon sediment permeability tensor (m^2);

μ Water dynamic viscosity (Pa·s);

ν_t Kynematic eddy viscosity ($\mathrm{m^2/s}$);

ρ Water density ($\mathrm{kg/m^3}$);

σ_k Closure coefficient (-);

σ_ω Closure coefficient (-);

τ Tortuosity factor (-);

τ_{ij} Reynolds stresses ($\mathrm{kg/(m \cdot s^2)}$);

θ Sediment porosity (-);

ω Specific dissipation ($\mathrm{s^{-1}}$).

Upper case

Γ_{DOC} DOC oxidation rate (mol/(L·s));

Γ_{nitr} Nitrification rate (mol/(L·s));

$\Gamma_{red,1}$ Oxygen reduction rate (mol/(L·s));

$\Gamma_{red,2}$ Nitrate reduction rate (mol/(L·s));

$\Gamma_{red,i}$ Reduction rate of the i-th electron acceptor (mol/(L·s)).

List of Figures

List of Tables

Bibliography

Aitkenhead-Peterson, J. A., Steele, M. K., Nahar, N., Santhy, K., DEC 2009. Dissolved organic carbon and nitrogen in urban and rural watersheds of south-central Texas: land use and land management influences. Biogeochemistry 96 (1-3), 119–129.

Alexander, M. D., Caissie, D., 2003. Variability and comparison of hyporheic water temperatures and seepage fluxes in a small atlantic salmon stream. Ground Water 41 (1), 72–82, 46.

Alexander, R. B., Smith, R. A., Schwarz, G. E., FEB 17 2000. Effect of stream channel size on the delivery of nitrogen to the Gulf of Mexico. Nature 403 (6771), 758–761.

Alley, W. M., Healy, R. W., LaBaugh, J. W., Reilly, T. E., June 2002. Flow and storage in groudwater systems. Science 296, 1985–1990.

Anderson, J. K., Wondzell, S. M., Gooseff, M. N., Haggerty, R., 2005. Patterns in stream longitudinal profiles and implications for hyporheic exchange flow at the h.j. andrews experimental forest, oregon, usa. Hydrological Processes 19 (15), 2931–2949, 46.

Angelier, E., 1953. Recherches écologiques et biogeographiques sur la fauna des sables submerges. Archs. Zool. exptl. gén 90, 37–162.

Angermann, L., Krause, S., Lewandowski, J., OCT 11 2012. Application of heat pulse injections for investigating shallow hyporheic flow in a lowland river. Water Resour. Res. 48.

Arnon, S., Gray, K. A., Packman, A. I., 2007. Biophysicochemical process coupling controls nitrate use by benthic biofilms. Limnol. Oceanogr. 52 (4), 1665–1671.

Bardini, L., Boano, F., Cardenas, M. B., Revelli, R., Ridolfi, L., 2012. Nutrient cycling in bedform induced hyporheic zones. Geochim. Cosmochim. Acta 84, 47–61.

Battin, T. J., Kaplan, L. A., Findlay, S., Hopkinson, C. S., Marti, E., Packman, A. I., Newbold, J. D., Sabater, F., 2008. Biophysical controls on organic carbon fluxes in fluvial networks. Nat. Geosci. 1 (2), 95–100.

Bear, J., Verruijt, A., 1992. Modeling Groundwater Flow and Pollution. D. Reidel Publishing Company, Dordrecht, Holland.

Bencala, K. E., 1984. Interactions of solutes and streambed sediment. 2. a dynamic analysis of coupled hydrologic and chemical processes that determine solute transport. Water Resour. Res. 20 (12), 1804–1814.

Bencala, K. E., 2005. Hyporheic exchange flow. In: Anderson, M. G., McDonnell, J. (Eds.), Encyclopedia of Hydrological Sciences. Vol. 3. Wiley: Chichester, Ch. 10, pp. 1733–1740.

Bencala, K. E., Walters, R. A., 1983. Simulation of solute transport in a mountain pool-and-riffle stream: a transient storage model. Water Resour. Res. 19 (3), 718–724.

Boano, F., Camporeale, C., Revelli, R., Ridolfi, L., 2006a. Sinuosity-driven hyporheic exchange in meandering rivers. Geophys. Res. Lett. 33.

Boano, F., Demaria, A., Revelli, R., Ridolfi, L., 2010. Biogeochemical zonation due to intrameander hyporheic flow. Water Resour. Res. 46.

Boano, F., Packman, A. I., Cortis, A., Revelli, R., Ridolfi, L., 2007a. A continuous time random walk approach to the stream transport of solutes. Water Resour. Res. 43.

80

Boano, F., Revelli, R., Ridolfi, L., 2006b. Stochastic modelling of do and bod components in a stream with random inputs. Adv. Water Resour. 29 (9), 1341–1350.

Boano, F., Revelli, R., Ridolfi, L., 2007b. Bedform-induced hyporheic exchange with unsteady flows. Adv. Water Resour. 30 (1), 148–156.

Boano, F., Revelli, R., Ridolfi, L., 2008. Reduction of the hyporheic zone volume due to the stream-aquifer interaction. Geophys. Res. Lett. 35.

Bohlke, J. K., Antweiler, R. C., Harvey, J. W., Laursen, A. E., Smith, L. K., Smith, R. L., Voytek, M. A., MAR 2009. Multiscale measurements and modeling of denitrification in streams with varying flow and nitrate concentration in the upper Mississippi River basin, USA. Biogeochemistry 93 (1-2), 117–141, Workshop on Denitrification Modeling Across Terrestrial, Freshwater, and Marine Systems, Inst Ecosyst Studies, Millbrook, NY, NOV 28-30, 2006.

Bottacin-Busolin, A., Marion, A., 2010. Combined role of advective pumping and mechanical dispersion on time scales of bed form–induced hyporheic exchange. Water Resour. Res. 46.

Bottacin-Busolin, A., Singer, G., Zaramella, M., Battin, T. J., Marion, A., 2009. Effects of streambed morphology and biofilm growth on the transient storage of solutes. Environ. Sci. Technol. 43 (19), 7337–7342.

Boudreau, B. P., AUG 2000. The mathematics of early diagenesis: From worms to waves. Rev. Geophys. 38 (3), 389–416.

Boulton, A. J., 1993. Stream ecology and surface hyporheic hydrologic exchange - implications, techniques and limitations. Australian Journal of Marine and Freshwater Research 44 (4), 553–564, 72.

Boulton, A. J., Findlay, S., Marmonier, P., Stanley, E. H., Valett, H. M., 1998. The functional significance of the hyporheic zone in streams and rivers. Annu. Rev. Ecol. Evol. Syst. 29, 59–81, 164.

Boyer, E. W., Howarth, R. W., Galloway, J. N., Dentener, F. J., Green, P. A., Vorosmarty, C. J., MAR 2 2006. Riverine nitrogen export from the continents to the coasts. Glob. Biogeochem. Cycle 20 (1).

Brunke, M., Gonser, T., 1997. The ecological significance of exchange processes between rivers and groundwater. Freshwater Biol. 37, 1–33.

Burkholder, B. K., Grant, G. E., Haggerty, R., Khangaonkar, T., Wampler, P. J., MAR 30 2008. Influence of hyporheic flow and geomorphology on temperature of a large, gravel-bed river, Clackamas River, Oregon, USA. Hydrol. Process. 22 (7), 941–953, General Assembly of the European-Geosciences-Union, Vienna, Austria, APR 15-20, 2007.

Cardenas, M., Cook, P., Jiang, Traykovski, H., 2008a. Constraining denitrification in permeable wave-influenced marine sediment using linked hydrodynamic and biogeochemical modeling. Earth Planet. Sc. Lett. 275, 127–137.

Cardenas, M., Wilson, J., 2007a. Effects of current-bed form induced fluid flow on the thermal regime of sediments. Water Resour. Res. 43.

Cardenas, M. B., 2008a. The effect of river bend morphology on flow and timescales of surface water-groundwater exchange across pointbars. J. Hydrol. 362 (1-2), 134–141.

Cardenas, M. B., 2008b. Surface water-groundwater interface geomorphology leads to scaling of residence times. Geophys. Res. Lett. 35 (8).

Cardenas, M. B., Wilson, J. L., 2007b. Dunes, turbulent eddies, and interfacial exchange with permeable sediments. Water Resour. Res. 43 (8), W08412.

Cardenas, M. B., Wilson, J. L., 2007c. Hydrodynamics of coupled flow above and below a sediment-water interface with triangular bedforms. Adv. Water Resour. 30, 301–313.

Cardenas, M. B., Wilson, J. L., Haggerty, R., 2008b. Residence time of bedform-driven hyporheic exchange. Adv. Water Resour. 31 (10), 1382–1386.

Cardenas, M. B., Wilson, J. L., Zlotnik, V. A., 2004. Impact of heterogeneity, bed forms, and stream curvature on subchannel hyporheic exchange. Water Resour. Res. 40.

Chappuis, P. A., 1942. Eine neue methode zur untersuchung der grundwasserfauna. In: Acta Scientifica Mathematisch. Vol. 6. University of Francio-Josephina, pp. 1–7.

COMSOL Multiphysics, COMSOL Multiphysics User's Guide. Burlington, Mass.

Council of the European Community (CEC), 2000. Directive 2000/60/EC of the European Parliament and of the Council of 23 October 2000 establishing a framework for community action in the field of water policy. In: Official Journal of the European Communities Vol. L327/1, pp. 1–72.

Danielopol, D. L., MAR 1989. Gorundwater fauna associated with riverine aquifers. J. N. Am. Benthol. Soc. 8 (1), 18–35.

De Smedt, F., 2006. Analytical solutions for transport of decaying solutes in rivers with transient storage. J. Hydrol. 330 (3-4), 672–680, de Smedt, F. 41.

De Smedt, F., JUN 10 2007. Analytical solution and analysis of solute transport in rivers affected by diffusive transfer in the hyporheic zone. J. Hydrol. 339 (1-2), 29–38.

Duff, J. H., Toner, B., Jackman, A. P., Avanzino, R. J., Triska, F. J., 2000. Determination of groundwater discharge into a sand and gravel bottom river: a comparison of chloride dilution and seepage meter techniques. Vol. 27 of International Association of theoretical and applied limnology - Proceedings. Int Assoc Theoret & Appl Limnol, pp. 406–411, 27th Congress of the International-Association-of-Theoretical-and-Applied-Limnology, Dublin, Ireland, 1998.

Durlofsky, L. J., 1991. Numerical calculation of equivalent grid block permeability tensors for heterogeneous porous media. Water Resour. Res. 27 (5), 699–708.
URL `http://dx.doi.org/10.1029/91WR00107`

Elliott, A. H., Brooks, N. H., 1997a. Transfer of nonsorbing solutes to a streambed with bed forms: Laboratory experiments. Water Resour. Res. 33 (1), 137–151, 17.

Elliott, A. H., Brooks, N. H., 1997b. Transfer of nonsorbing solutes to a streambed with bed forms: Theory. Water Resour. Res. 33 (1), 123–136, 31.

Endreny, T., Lautz, L., Siegel, D. I., FEB 12 2011. Hyporheic flow path response to hydraulic jumps at river steps: Flume and hydrodynamic models. Water Resour. Res. 47.

Eylers, H., Brooks, N. H., Morgan, J. J., 1995. Transport of adsorbing metals from stream water to a stationary sand-bed in a laboratory flume. Mar. Freshw. Res. 46 (1), 209–214, 6th International Symposium of the International-Association-for-Sediment-Water-Sciences, Santa Barbara, CA, DEC, 1993.

Findlay, S., 1995. Importance of surface-subsurface exchange in stream ecosystems: the hyporhei zone. Limnol. Oceanogr. 40 (1), 159–164, 43.

Fischer, H., Kloep, F., Wilzcek, S., Pusch, M. T., 2005. A river's liver - microbial processes within the hyporheic zone of a large lowland river. Biogeochemistry 76 (2), 349–371, 70.

Fischer, H., Pusch, M., 2001. Comparison of bacterial production in sediments, epiphyton and the pelagic zone of a lowland river. Freshwater Biol. 46 (10), 1335–1348, 77.

Fleckenstein, J. H., Krause, S., Hannah, D. M., Boano, F., 2010. Groundwater-surface water interactions: New methods and models to improve understanding of processes and dynamics. Advances In Water Resources 33 (11), 1291–1295.

Francis, B. A., Francis, L. K., Cardenas, M. B., 2010. Water table dynamics and groundwater-surface water interaction during

filling and draining of a large fluvial island due to dam-induced river stage fluctuations. Water Resources Research 46, W07513.

Fuller, C. C., Harvey, J. W., 2000. Reactive uptake of trace metals in the hyporheic zone of a mining-contaminated stream, pinal creek, arizona. Environ. Sci. Technol. 34 (7), 1150–1155, 27.

Gandy, C. J., Smith, J. W. N., Jarvis, A. P., 2007. Attenuation of mining-derived pollutants in the hyporheic zone: A review. Sci. Total Environ. 373 (2-3), 435–446, gandy, C. J. Smith, J. W. N. Jarvis, A. P. 49.

Genereux, D. P., Leahy, S., Mitasova, H., Kennedy, C. D., Corbett, D. R., SEP 5 2008. Spatial and temporal variability of streambed hydraulic conductivity in West Bear Creek, North Carolina, USA. J. Hydrol. 358 (3-4), 332–353.

Gomez, J. D., Wilson, J. L., Cardenas, M. B., SEP 20 2012. Residence time distributions in sinuosity-driven hyporheic zones and their biogeochemical effects. Water Resour. Res. 48 (9), 1–17.

Gooseff, M. N., Anderson, J. K., Wondzell, S., LaNier, J., Haggerty, R., 2006. A modeling study of hyporheic exchange pattern and the sequence, size, and spacing of stream bedforms in mountain stream networks, oregon, usa (retraction of vol 19, pg 2915, 2005). Hydrological Processes 20 (11), 2441–+, gooseff, M. N. Anderson, J. K. Wondzell, S. M. LaNier, J. Haggerty, R. 35.

Gooseff, M. N., Briggs, M. A., Bencala, K. E., McGlynn, B. L., Scott, D. T., 2013. Do transient storage parameters directly scale in longer, combined stream reaches? reach length dependence of transient storage interpretations. J. Hydrol. 483, 16–25.

Gu, C., Hornberger, G. M., Mills, A. L., Herman, J. S., Flewelling, S. A., DEC 28 2007. Nitrate reduction in streambed sediments: Effects of flow and biogeochemical kinetics. Water Resour. Res. 43 (12).

Haggerty, R., Wondzell, S. M., Johnson, M. A., 2002. Power-law residence time distribution in the hyporheic zone of a 2nd-order mountain stream. Geophys. Res. Lett. 29 (13).

Harvey, J., Wagner, B., 2000. Streams and Ground Waters. Academic, San Diego, Calif., Ch. Quantifying hydrologic interactions between streams and their subsurface hyporheic zones, pp. 4–44.

Harvey, J. W., Bencala, K. E., 1993. The effect of streambed topography on surface-subsurface water exchange in mountain catchments. Water Resour. Res. 29 (1), 89–98.

Harvey, J. W., Fuller, C. C., 1998. Effect of enhanced manganese oxidation in the hyporheic zone on basin-scale geochemical mass balance. Water Resour. Res. 34 (4), 623–636.

Hatch, C. E., Fisher, A. T., Revenaugh, J. S., Constantz, J., Ruehl, C., OCT 11 2006. Quantifying surface water-groundwater interactions using time series analysis of streambed thermal records: Method development. Water Resour. Res. 42 (10).

Hatch, C. E., Fisher, A. T., Ruehl, C. R., Stemler, G., AUG 11 2010. Spatial and temporal variations in streambed hydraulic conductivity quantified with time-series thermal methods. J. Hydrol. 389 (3-4), 276–288.

Hedin, L. O., von Fischer, J. C., Ostrom, N. E., Kennedy, B. P., Brown, M. G., Robertson, G. P., 1998. Thermodynamic constraints on nitrogen transformations and other biogeochemical processes at soil-stream interfaces. Ecology 79 (2), 684–703, 89.

Hunter, K. S., Wang, Y., Van Cappellen, P., 1998. Kinetic modeling of microbially-driven redox chemistry of subsurface environments: coupling transport, microbial metabolism and geochemistry. J. Hydrol. 209, 53–80.

Jin, G., Tang, H., Gibbes, B., Li, L., Barry, D. A., NOV 2010. Transport of nonsorbing solutes in a streambed with periodic bedforms. Adv. Water Resour. 33 (11, SI), 1402–1416.

Jones, J. B., Mulholland, P. J. (Eds.), 2000. Streams and Ground Waters. Academic, San Diego, Calif.

Jonsson, N., 1991. Influence of water flow, water temperature and light on fish migration in rivers. Nordic J. Freshw. Res. 60, 20–35.

Kaeser, D., APR 2010. A new habitat of subsurface waters: the hyporheic biotope. Fundam. Appl. Limnol. 176 (4), 291–302.

Kalbus, E., Schmidt, C., Molson, J. W., Reinstorf, F., Schirmer, M., 2009. Influence of aquifer and streambed heterogeneity on the distribution of groundwater discharge. Hydrol. Earth Syst. Sci. 13 (1), 69–77.

Kasahara, T., Wondzell, S. M., 2003. Geomorphic controls on hyporheic exchange flow in mountain streams. Water Resour. Res. 39 (1).

Keery, J., Binley, A., Crook, N., Smith, J. W. N., 2007. Temporal and spatial variability of groundwater-surface water fluxes: Development and application of an analytical method using temperature time series. J. Hydrol. 336 (1-2), 1–16, keery, John Binley, Andrew Crook, Nigel Smith, Jonathan W. N. 62.

Kessler, A. J., Glud, R. N., Cardenas, M. B., Larsen, M., Bourke, M. F., Cook, P. L. M., 2012. Quantifying denitrification in rippled permeable sands through combined flume experiments and modeling. Limnol. Oceanogr. 57 (4), 1217–1232.

Krause, S., Blume, T., Cassidy, N. J., 2012. Investigating patterns and controls of groundwater up-welling in a lowland river by combining Fibre-optic Distributed Temperature Sensing with observations of vertical hydraulic gradients. Hydrol. Earth Syst. Sci. 16 (6), 1775–1792.

Krause, S., Hannah, D. M., Fleckenstein, J. H., Heppell, C. M., Kaeser, D., Pickup, R., Pinay, G., Robertson, A. L., Wood, P. J., JUL 2011. Inter-disciplinary perspectives on processes in the hyporheic zone. Ecohydrology 4 (4, SI), 481–499.

Krause, S., Heathwaite, L., Binley, A., Keenan, P., 2009. Nitrate concentration changes at the groundwater-surface water interface of a small cumbrian river. Hydrol. Process. 23 (15), 2195–2211.

Lautz, L., Fanelli, R., 2008. Seasonal biogeochemical hotspots in the streambed around restoration structures. Biogeochemistry 91 (1), 85–104.

Lautz, L. K., Ribaudo, R. E., NOV 2012. Scaling up point-in-space heat tracing of seepage flux using bed temperatures as a quantitative proxy. Hydrogeol. J. 20 (7), 1223–1238.

Malard, F., Tockner, K., Dole-Olivier, M.-J., Ward, J. V., 2002. A landscape perspective of surface-subsurface hydrological exchanges in river corridors. Freshwater Biol. 47, 621–640.

Marion, A., Bellinello, M., Guymer, I., Packman, A., 2002. Effect of bed form geometry on the penetration of nonreactive solutes into a streambed. Water Resour. Res. 38 (10).

Marion, A., Packman, A. I., Zaramella, M., Bottacin-Busolin, A., SEP 25 2008a. Hyporheic flows in stratified beds. Water Resour. Res. 44 (9).

Marion, A., Zaramella, M., 2005. Diffusive behavior of bedform-induced hyporheic exchange in rivers. J. Envir. Eng. 131 (9), 1260–1266.

Marion, A., Zaramella, M., Bottacin-Busolin, A., OCT 14 2008b. Solute transport in rivers with multiple storage zones: The STIR model. Water Resour. Res. 44 (10).

Marion, A., Zaramella, M., Packman, A. I., 2003. Parameter estimation of the transient storage model for stream-subsurface exchange. J. Environ. Eng. 129 (5), 456–463.

Marzadri, A., Tonina, D., Bellin, A., SEP 20 2012. Morphodynamic controls on redox conditions and on nitrogen dynamics within the hyporheic zone: Application to gravel bed rivers with alternate-bar morphology. J. Geophys. Res. 117.

Marzadri, A., Tonina, D., Bellin, A., Vignoli, G., Tubino, M., 2010. Semianalytical analysis of hyporheic flow induced by alternate bars. Water Resources Research 46.

McClain, M. E., Boyer, E. W., Dent, C. L., Gergel, S. E., Grimm, N. B., Groffman, P. M., Hart, S. C., Harvey, J. W., Johnston, C. A., Mayorga, E., McDowell, W. H., Pinay, G., 2003. Biogeochemical hot spots and hot moments at the interface of terrestrial and aquatic ecosystems. Ecosystems 6 (4), 301–312.

Montroll, E. W., Weiss, G. H., 1965. Random walks on lattices. II. J. Math. Phys. 6 (2), 167–181.

Mulholland, P. J., Helton, A. M., Poole, G. C., Hall, R. O., Hamilton, S. K., Peterson, B. J., Tank, J. L., Ashkenas, L. R., Cooper, L. W., Dahm, C. N., Dodds, W. K., Findlay, S. E. G., Gregory, S. V., Grimm, N. B., Johnson, S. L., McDowell, W. H., Meyer, J. L., Valett, H. M., Webster, J. R., Arango, C. P., Beaulieu, J. J., Bernot, M. J., Burgin, A. J., Crenshaw, C. L., Johnson, L. T., Niederlehner, B. R., O'Brien, J. M., Potter, J. D., Sheibley, R. W., Sobota, D. J., Thomas, S. M., 2008. Stream denitrification across biomes and its response to anthropogenic nitrate loading. Nature 452 (7184), 202–206.

Murdoch, L. C., Kelly, S. E., JUN 24 2003. Factors affecting the performance of conventional seepage meters. Water Resour. Res. 39 (6).

Naegeli, M. W., Uehlinger, U., 1997. Contribution of the hyporheic zone to ecosystem metabolism in a prealpine gravel-bed river. Journal of the North American Benthological Society 16 (4), 794–804, 43.

O'Connor, B. L., Hondzo, M., 2008. Dissolved oxygen transfer to sediments by sweep and eject motions in aquatic environments. Limnol. Oceanogr. 53 (2), 566–578.

O'Connor, D. J., MAY/JUNE 1988. Models of sorptive toxic substances in freshwater systems. i. basic equations. Journal of Environmental Engineering 114 (3), 507–532.

Orghidan, T., 1959. Ein neuer lebensraum des unterirdischen wassers: der hyporheische biotop. Arch. Hydrobiol. 55, 392–414.

Packman, A., Salehin, M., Zaramella, M., 2004. Hyporheic exchange with gravel beds: Basic hydrodynamic interactions and bedform-induced advective flows. J. Hydraul. Eng. – ASCE 130 (7), 647–656, 25.

Packman, A. I., Brooks, N. H., 2001. Hyporheic exchange of solutes and colloids with moving bed forms. Water Resour. Res. 37 (10), 2591–2605, 69.

Packman, A. I., Brooks, N. H., Morgan, J. J., 2000. A physico-chemical model for colloid exchange between a stream and a sand streambed with bed forms. Water Resour. Res. 36 (8), 2351–2361.

Palmer, M. A., 1993. Experimentation in the hyporheic zone - challenges and prospectus. J. N. Am. Benthol. Soc. 12 (1), 84–93.

Pinay, G., O'Keefe, T. C., Edwards, R. T., Naiman, R. J., MAY 2009. Nitrate removal in the hyporheic zone of a salmon river in alaska. River Res. Appl. 25 (4), 367–375.

Poole, G. C., Stanford, J. A., Running, S. W., Frissell, C. A., 2006. Multiscale geomorphic drivers of groundwater flow paths: subsurface hydrologic dynamics and hyporheic habitat diversity. Journal of the North American Benthological Society 25 (2), 288–303, 57.

Prchalova, M., Horky, P., Slavik, O., Vetesnik, L., Halacka, K., 2011. Fish occurrence in the fishpass on the lowland section of the river elbe, czech republic, with respect to water temperature, water flow and fish size. Folia Zool. 60 (2), 104–114.

Precht, E., Franke, U., Polerecky, L., Huettel, M., MAY 2004. Oxygen dynamics in permeable sediments with wave-driven pore water exchange. Limnol. Oceanogr. 49 (3), 693–705.

Puckett, L. J., Zamora, C., Essaid, H., Wilson, J. T., Johnson, H. M., Brayton, M. J., Vogel, J. R., MAY-JUN 2008. Transport and fate of nitrate at the ground-water/surface-water interface. J. Environ. Qual. 37 (3), 1034–1050.

Qian, Q., Voller, V. R., Stefan, H. G., 2008. A vertical dispersion model for solute exchange induced by underflow and periodic hyporheic flow in a stream gravel bed. Water Resour. Res. 44 (7), W07422.

Revelli, R., Boano, F., Camporeale, C., Ridolfi, L., 2008. Intra-meander hyporheic flow in alluvial rivers. Water Resources Research 44 (12), W12428.

Rosenberry, D. O., Klos, P. Z., Neal, A., FEB 15 2012. In situ quantification of spatial and temporal variability of hyporheic exchange in static and mobile gravel-bed rivers. Hydrolog. Process. 26 (4), 604–612.

Rosenberry, D. O., Pitlick, J., NOV 15 2009. Local-scale variability of seepage and hydraulic conductivity in a shallow gravel-bed river. Hydrolog. Process. 23 (23), 3306–3318.

Runkel, R. L., McKnight, D. M., Andrews, E. D., 1998. Analysis of transient storage subject to unsteady flow: diel flow variation in an antarctic stream. Journal of the North American Benthological Society 17 (2), 143–154, 32.

Saenger, N., Kitanidis, P. K., Street, R. L., 2005. A numerical study of surface-subsurface exchange processes at a riffle-pool pair in the lahn river, germany. Water Resour. Res. 41 (12).

Salehin, M., Packman, A. I., Paradis, M., 2004. Hyporheic exchange with heterogeneous streambeds: Laboratory experiments and modeling. Water Resour. Res. 40.

Salehin, M., Packman, A. I., Wörman, A., 2003. Comparison of transient storage in vegetated and unvegetated reaches of a small agricultural stream in Sweden: Seasonal variation and anthropogenic manipulation. Adv. Water Resour. 26, 951–964.

Savant, S. A., Reible, D. D., Thibodeaux, L. J., 1987. Convective transport within stable river sediments. Water Resour. Res. 23 (9), 1763–1768.

Sawyer, A. H., Cardenas, M. B., 2009. Hyporheic flow and residence time distributions in heterogeneous cross-bedded sediment. Water Resour. Res. 45, W08406.

Scher, H., Lax, M., 1973. Stochastic transport in a disordered solid. I. Theory. Phys. Rev. B 7, 4491–4502.

Schwoerbel, J., 1964. Die bedeutung des hyporheals für die benthische lebensgemeinschaft der flie?gewasser. Verhandlungen der Internationalen Limnologie 15, 215–226.

Smith, J. W. N., July 2005. Groundwater - surface water interactions in the hyporheic zone. Environment Agency Science Report SC030155/1, Environment Agency, Bristol, UK.

Smith, J. W. N., Bonell, M., Gibert, J., McDowell, W. H., Sudicky, E. A., Turner, J. V., Harris, R. C., JAN 2008. Groundwater-surface water interactions, nutrient fluxes and ecological response in river corridors: Translating science into effective environmental management. Hydrol. Process. 22 (1), 151–157.

Song, J. X., Chen, X. H., Cheng, C., Summerside, S., Wen, F. J., 2007. Effects of hyporheic processes on streambed vertical hydraulic conductivity in three rivers of nebraska. Geophys. Res. Lett. 34 (7), 5, song, Jinxi Chen, Xunhong Cheng, Cheng Summerside, Scott Wen, Fujiang 26.

Stanford, J. A., Ward, J. V., 1988. The hyporheic habitat of river ecosystems. Nature 335 (6185), 64–66, 18.

Stanford, J. A., Ward, J. V., 1993. An ecosystem perspective of alluvial rivers: connectivity and the hyporheic corridor. J. N. Am. Benthol. Soc. 12 (1), 48–60.

Stonedahl, S. H., Harvey, J. W., Worman, A., Salehin, M., Packman, A. I., 2010. A multiscale model for integrating hyporheic exchange from ripples to meanders. Water Resour. Res. 46.

Storey, R. G., Fulthorpe, R. R., Williams, D. D., 1999. Perspectives and predictions on the microbial ecology of the hyporheic zone. Freshwater Biol. 41 (1), 119–130, 64.

Tidwell, V., Wilson, J., AUG 2000. Heterogeneity, permeability patterns, and permeability upscaling: Physical characterization of a block of massillon sandstone exhibiting nested scales of heterogeneity. SPE Reserv. Eval. Eng. 3 (4), 283–291.

Tonina, D., Buffington, J. M., 2007. Hyporheic exchange in gravel bed rivers with pool-riffle morphology: Laboratory experiments and three-dimensional modeling. Water Resour. Res. 43 (1).

Tonina, D., Buffington, J. M., 2009. Hyporheic exchange in mountain rivers I: mechanics and environmental effects. Geog.

Compass 3 (3), 1063–1086.
URL http://dx.doi.org/10.1111/j.1749-8198.2009.00226.x

Triska, F. J., Kennedy, V. C., Avanzino, R. J., Zellweger, G. W.,
Bencala, K. E., 1989. Retention and transport of nutrients in a
third-order stream in Northwestern California: Hyporheic pro-
cesses. Ecology 70 (6), 1893–1905.

VanCappellen, P., Wang, Y. F., MAR 1996. Cycling of iron and
manganese in surface sediments: a general theory for the coupled
transport and reaction of carbon, oxygen, nitrogen, sulfur, iron,
and manganese. Am. J. Sci. 296 (3), 197–243.

Vervier, P., Gibert, J., Marmonier, P., Dole-Olivier, M.-J., 1992.
A perspective on the permeability of the surface freshwater-
groundwater ecotone. J. N. Am. Benthol. Soc. 11 (1), 93–102.

Westhoff, M. C., Gooseff, M. N., Bogaard, T. A., Savenije, H.
H. G., OCT 12 2011. Quantifying hyporheic exchange at high
spatial resolution using natural temperature variations along a
first-order stream. Water Resour. Res. 47.

Wilcox, D. C., 1991. A half century historical review of the k-w
model. AIAA Paper.

Williams, D. D., Febria, C. M., Wong, J. C. Y., APR 2010. Eco-
tonal and other properties of the Hyporheic Zone. Fundam. Appl.
Limnol. 176 (4), 349–364.

Williams, D. D., Hynes, H. B. N., 1974. The occurrence of bethos
deep in the substratum of a stream. Freshwat. Biol. 4, 233–256.

Woessner, W. W., 2000. Stream and fluvial plain ground water
interactions: Rescaling hydrogeologic thought. Ground Water
38 (3), 423–429, 71.

Wondzell, S. M., 2006. Effect of morphology and discharge on
hyporheic exchange flows in two small streams in the Cascade
Mountains of Oregon, USA. Hydrol. Process. 20 (2), 267–287,
46.

Wondzell, S. M., OCT 2011. The role of the hyporheic zone across
stream networks. Hydrol. Process. 25 (2), 3525–3532.

Wondzell, S. M., Gooseff, M. N., McGlynn, B. L., MAR 15 2010. An analysis of alternative conceptual models relating hyporheic exchange flow to diel fluctuations in discharge during baseflow recession. Hydrol. Proc. 24 (6), 686–694.

Wörman, A., Packman, A. I., Marklund, L., Harvey, J. W., Stone, S. H., APR 4 2007. Fractal topography and subsurface water flows from fluvial bedforms to the continental shield. Geophys. Res. Lett. 34 (7).

Wroblicky, G. J., Campana, M. E., Valett, H. M., Dahm, C. N., 1998. Seasonal variations in surface-subsurface water exchange and lateral hyporheic area of two stream-aquifer systems. Water Resour. Res. 34 (3), 317–328.

Zaramella, M., Packman, A. I., Marion, A., 2003. Application of the transient storage model to analyze advective hyporheic exchange with deep and shallow sediments. Water Resour. Res. 39 (7).

Zarnetske, J. P., Gooseff, M. N., Bowden, W. B., Greenwald, M. J., Brosten, T. R., Bradford, J. H., McNamara, J. P., 2008. Influence of morphology and permafrost dynamics on hyporheic exchange in arctic headwater streams under warming climate conditions. Geophys. Res. Lett. 35.

Zarnetske, J. P., Haggerty, R., Wondzell, S. M., Baker, M. A., MAR 2011. Dynamics of nitrate production and removal as a function of residence time in the hyporheic zone. J. Geophys. Res.-Biogeo. 116.

Zarnetske, J. P., Haggerty, R., Wondzell, S. M., Bokil, V. A., Gonzalez-Pinzon, R., 2012. Coupled transport and reaction kinetics control the nitrate source-sink function of hyporheic zones. Water Resour. Res. 48 (11).